

Characterization of Conjugated Polymer Actuation under Cerebral Physiological Conditions

Eugene Dariush Daneshvar¹ and Elisabeth Smela^{2*}

¹Department of Biomedical Engineering, University of Michigan, Ann Arbor, MI 48109

²Department of Mechanical Engineering, University of Maryland, College Park, MD 20742
smela@umd.edu

ABSTRACT

Conjugated polymer actuators have potential use in implantable neural interface devices for modulating the position of electrode sites within brain tissue or guiding insertion of neural probes along curved trajectories. The actuation of polypyrrole (PPy) doped with dodecylbenzenesulfonate (DBS) was characterized to ascertain whether it could be employed in the cerebral environment. Microfabricated bilayer beams were electrochemically cycled at either 22 or 37 °C in aqueous NaDBS or in artificial cerebrospinal fluid (aCSF). Nearly all the ions in aCSF were exchanged into the PPy – the cations Na⁺, K⁺, Mg²⁺, Ca²⁺, as well as the anion PO₄³⁻; Cl⁻ was not present. Nevertheless, deflections in aCSF were comparable to those in NaDBS and they were monotonic with oxidation level: strain increased upon reduction, with no reversal of motion despite the mixture of ionic charges and valences being exchanged. Actuation depended on temperature. Upon warming, the cyclic voltammograms showed additional peaks and an increase of 70% in the consumed charge. Bending was, however, much less affected: strain increased somewhat (6-13%) but remained monotonic, and deflections shifted (up to 20%). These results show how the actuation environment must be taken into account, and demonstrate proof of concept for actuated implantable neural interfaces.

Keywords: movable electrodes; conducting polymers; brain-machine interface; bilayers

1 INTRODUCTION

Conjugated polymers are a class of so-called “intelligent” materials because they respond to electrical stimuli and to their external environments. One response is a change in volume, which has led to their use as actuators. Several factors make such actuators promising for biomedical applications, as reviewed in [1], and there have been demonstrations of this, both in vitro and in vivo

* Corresponding author.

[2-6]. Conjugated polymers have been shown to be biocompatible [7-9], and their low actuation voltages (< 1 V) are considered benign for interactions with biological tissues [3, 9, 10]. These actuators can exert substantial forces [11, 12] because of their high elastic moduli (0.1 – 100 GPa) [1, 13]. In addition, they can be readily integrated with standard microfabrication processes [14].

For actuation, polypyrrole (PPy) is one of the most commonly used conjugated polymers. In our laboratory, we have often used PPy doped with dodecylbenzenesulfonate, PPy(DBS). The immunoreactivity of PPy(DBS) has previously been shown by histological testing to be favorable [3, 9, 10]. Although gradually degraded by operation in aqueous electrolytes, PPy(DBS) is stable for short-term use (up to several thousand cycles) [15].

Motivating the work presented here is the possibility of augmenting implantable neural interface devices with controllable bending elements. Adjusting the position of electrode sites within neural tissue to change electrode proximity to particular neurons may be beneficial for several reasons. For neural recording devices, the ability to move the electrode out of a damaged region may result in increased signal to noise ratios (SNR) [16]. For neural stimulating devices, more accurate electrode placement may increase treatment efficacy and lower the charge injection required for stimulation [17, 18]. In addition, actuators may be used to guide the insertion of neural probe devices, allowing non-straight trajectories and active steering to target structures with precision, as needed for deep brain stimulation therapy [19]. Therefore, it is critical to understand the expected behavior of the actuator in the cerebral environment.

We have previously demonstrated the feasibility of using PPy(DBS) to controllably bend neural electrodes within an agarose brain phantom during their insertion (Figure 1) [20]. Figure 1a shows an array of 5 probes immediately after fabrication; the beams are bent due to residual stress. The electrode beams in Figure 1b were actuated within the brain phantom (0.5% agarose and 0.1 M NaDBS), which has a stiffness similar to brain tissue. The PPy(DBS) produced sufficient force to move the electrodes out of plane during insertion into the gel, as required for cortical applications. Other applications, such as electrodes for the eye or ear, would operate in aqueous environments and encounter smaller opposing forces. Probes may also be bent at segments acting as joints (Figure 1c), rather than along the entire length. These results were promising for the potential use of conjugated polymers in neural interface devices.

In this paper we characterize the behavior of the actuators, studying them at body temperature (37 °C) in artificial cerebrospinal fluid (aCSF), which contains a mixture of ions. Actuation in NaDBS at room temperature (22 °C) is used as a comparison because extensive prior characterization has been performed in this electrolyte [21-23]. We show that the performance is substantially the same, demonstrating that these actuators may be used under physiological conditions.

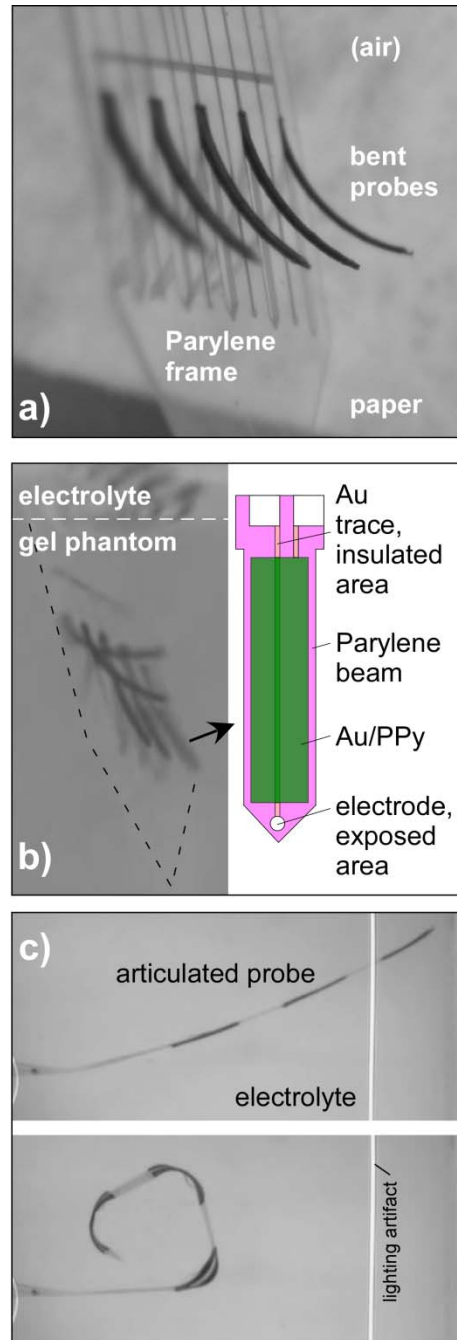


Figure 1. a) An array of 5 probe devices in air having lengths of 1 mm and widths between 50 μm and 250 μm , deflected out of plane with uniform curvature after fabrication, with no applied voltage. b) A similar set of probes with lengths of 800 μm actuated during penetration into a gel brain tissue phantom. The Parylene probe beams included an insulated electrode trace with an exposed Au electrode site at the tip and an overlying PPy/Au actuator. c) A segmented beam with actuators at three joints, electrochemically reduced to be straight (top) and oxidized to be bent (bottom) in NaDBS solution.

Actuation strain in aCSF was somewhat smaller than in NaDBS (by a factor of 0.89 at room temperature), and approximately the same charge density was exchanged (102%). Increasing the temperature to 37 °C resulted in a small increase in the actuation strain (by 13% in NaDBS and 6% in aCSF), but also a significant increase in the exchanged charge (by ~67% in both cases). Elemental analysis showed that in addition to Na, samples cycled in aCSF contained Mg, Ca, K, P and O (from PO_4^{3-} and its protonated forms), but no Cl. Despite the substantial amount of PO_4^{3-} , the actuation remained monotonic with voltage and did not reverse due to anion ingress and egress.

1.1 Conjugated polymer actuators

Conjugated polymers such as polypyrrole are characterized by alternating single and double bonds between the carbon atoms along the polymer backbone [1, 24]. Mobile positive charges are produced when electrons are removed from the charge-neutral polymer (i.e., when the polymer is oxidized), making the material electrically conducting. PPy is electro-polymerized in the oxidized (“doped”) state. Therefore, to maintain overall charge neutrality during film deposition, negatively charged anions are incorporated into the matrix. A large number of anions are incorporated: one for every 3-4 pyrrole units [25]. The anions therefore strongly influence the structure of the material, and thus the mechanical and electrical properties. It is thus necessary to specify the anion used during deposition when naming the polymer; PPy(DBS) and PPy(ClO_4) have quite different microstructures and behaviors.

Oxidation can be achieved electrochemically, and it is reversible: applying a sufficiently negative potential returns the electrons to the polymer, reducing it to the neutral state. To maintain charge neutrality in the material, the dopant anions are expelled into the surrounding electrolyte, if the anions are small enough (such as ClO_4^-); these are anion-exchanging polymers. Alternatively, if the anions that were incorporated during polymerization are too large to exit (such as DBS^-) and are thus entrapped in the polymer, then during reduction cations are pulled in by the electrostatic forces (cation-exchanging polymers). The exit or influx of ions, each surrounded by a “shell” of solvent (which is water in biomedical applications), causes a change in polymer volume that can be harnessed to perform mechanical work. (It also results in a change in the elastic modulus as a function of oxidation level [23, 26].)

The actuation strain is the change in length divided by original length, $\Delta L/L$, that would occur in a free-standing film due to redox. It is positive upon ion and solvent influx, and its magnitude depends on the number of solvent molecules accompanying the ion in its solvation shell. In cation-exchanging materials, lower atomic weight cations, which have a higher charge density and are thus surrounded by larger hydration shells [27], produce greater force [28] and displacement [21, 28, 29].

Divalent cations interact more strongly with the polymer than monovalent cations, and they have a lower mobility [22]. In other systems, they have been shown to electrostatically crosslink ionic polymer chains [30]. Divalent cations may require a stronger driving force (electrochemical potential) for insertion into or expulsion from the conjugated polymer [31] and result in less expansion during polymer reduction [32].

PPy(DBS) is one example of a cation-exchanging material, and it has been previously characterized in some depth upon cycling in aqueous NaCl and NaDBS. In aqueous solutions containing Na⁺, the actuation strain α in the plane of the film (inplane, i.e. parallel to the surface) is approximately 3% in the bulk [21, 33]. The inplane actuation strain is what leads to bending in bilayer actuators. (The out of plane actuation strain (perpendicular to the surface) in thin films can be ten times larger [34].)

Small anions, such as Cl⁻, may also participate in charge balance in PPy(DBS), becoming incorporated during oxidation and ejected during reduction [32, 35-37]. These typically have a different mobility in the polymer than the cations and a different potential window in which they are exchanged. The simultaneous transport of anions and cations in opposite directions at different speeds can result in a reversal in the strain direction [38-40]. Non-monotonic motion is problematic for control over actuator position.

Temperature has also been found to play a role in actuation. Actuators operating at elevated temperatures showed greater strain [41, 42] and accelerated creep [43].

Conjugated polymer actuator performance therefore depends not only on the synthesis medium, but also on the medium in which it is employed. Because the roles of the electrolyte and the temperature are not yet fully understood, new operation conditions must be characterized in terms of critical performance characteristics such as actuation strain, actuation stress (or, in the case of bending bilayers, moment), and speed. In this paper we characterize actuation strain. (Some information on speed has been included in the Supporting Information.)

1.2 Actuation in cerebral physiological ion concentrations and temperature

The prior demonstrations of biomedical applications [2-6] did not characterize actuation strain or deflection in those media. PPy(DBS) actuation has, however, been tested in several ionic solutions and temperature ranges. The majority of these studies have been done by systematically cycling one cation at a time [41, 44, 45] or by cycling in a solution with a single anion and cation, such as NaCl [46, 47]. PPy(DBS) has not yet been characterized in the ionic mixture and temperature found in the brain. For the long-term goal of producing movable neural interfaces, performance in cerebrospinal fluid (CSF) at body temperature needs to be determined. Ion concentrations in CSF are listed in Table 1. The primary constituents are Na⁺ and Cl⁻. CSF also contains glucose, proteins (430 mg/L), and lymphocytes (< 4 μm^3), and it is maintained at a pH of 7.31 [48, 49]. Artificial cerebrospinal fluid (aCSF) is used in lab settings to match the electrolyte concentrations of CSF, but it lacks the other components. This study examined the effects of the mixed ionic components of CSF on actuation, but future work will need to examine the effects of the other components, also.

Table 1. Ionic components of artificial cerebrospinal fluid [48].

CSF Ionic Component		Hydrated Radius (pm) [27]	Concentration (mM)
Sodium	Na ⁺	450	135-150
Chlorine	Cl ⁻	300	115-130
Potassium	K ⁺	300	2.6-3.0
Calcium	Ca ²⁺	600	1.0-1.4
Magnesium	Mg ²⁺	800	1.2-1.5
Phosphate	*PO ₄ ³⁻	400	0.4-0.6

* The charge depends on pH, going from PO₄³⁻ at high pH to H₃PO₄ at low pH.

2 METHODS

2.1 Bilayer beam actuator fabrication

Devices were fabricated using standard photolithography techniques (Lurie Nanofabrication Facility, University of Michigan). They consisted of a PPy/Au bilayer on a Parylene substrate, with no probe electrode. Photoresist (Shipley 1813, AZ Electronic Materials) was spin-coated onto a 4" silicon wafer and baked at 95 °C for 90 minutes to serve as a final release layer. Parylene C was deposited over the resist ($12.9 \pm 0.8 \mu\text{m}$, PDS 2035, Specialty Coating Systems), and after an oxygen plasma clean (PlasmaTherm 790, 150 mT, 99 sccm O₂, 100 W, 30 sec), chromium (Cr, 150 Å) and gold (Au, 1500 Å) were evaporated (Enerjet Evaporator, 2×10^{-6} T, 10 Å/sec) onto the Parylene. A second layer of photoresist was deposited and patterned using a Cr/glass mask to define the (identical) metal and beam shapes. The metal layers were patterned by wet etching (Transene TFA Au etchant, CR-14 Cr etchant). The Parylene was dry etched using an oxygen plasma (conditions as above, 200 nm/min etch rate), employing the resist and the metal as a mask. The beams were released by soaking the wafers in acetone, thereby dissolving the first resist layer. They were $13.1 \pm 0.8 \mu\text{m}$ thick, 10 mm long, and 0.5 mm wide. The beams were rinsed in isopropanol and water and allowed to air dry before use.

PPy(DBS) was polymerized galvanostatically (at constant current) to a thickness of $11.3 \pm 0.8 \mu\text{m}$ onto the Au surface in a solution of 0.1 M pyrrole (Aldrich) and 0.1 M NaDBS (Aldrich) in deionized (DI) water using a galvanostat/potentiostat (Ecochemie Autolab PGStat 12). The deposition current density was 1 mA/cm². (Polymerizing at higher currents has been shown to reduce actuation strain [50-52].) A porous carbon counter electrode and Ag/AgCl reference electrode (Bioanalytical Systems Inc.) were used during polymerization. Samples were rinsed in DI water and allowed to dry at ambient conditions for at least 24 hours. Parylene and PPy thicknesses were measured using scanning electron microscopy (SEM) images (Philips XL30ESEM, 5 kV) of

beam cross-sections. Bilayer devices were stored in closed Petri dishes lined with cleanroom paper wipes.

2.2 Actuator cycling

Electrochemical cycling took place in four conditions: in 0.15 M NaDBS or in aCSF (see Table 1) at either 22 or 37 °C. The counter electrode was a 1x1” platinum foil and the reference electrode was a dedicated Ag/AgCl reference electrode used only for cycling. The counter and reference electrodes were rinsed in water between different solutions.

The positive charge density (C/m^3) consumed during oxidation was found by integrating the current over the time of the forward sweep from -1.0 V to +0.4 V and dividing by the measured PPy volume; the negative charge density during reduction was found analogously, and the total charge density was taken as the sum of the absolute values. (I.e., energy recovery was not considered.)

2.3 Beam tip deflection, curvature, and actuation strain

Digital video of bilayer actuation was recorded through a microscope (Leica, 10x zoom) at 30 frames per second (Pinnacle Dazzle DVC 100 digital video recorder). Image frames were extracted from the video and sampled every 10 frames, resulting in 3 frames per second (Quicktime 7 Pro, Apple Inc.). Device dimensions were used for image size calibration. Positional resolution was 22 $\mu\text{m}/\text{pixel}$.

Three frames are shown overlaid in Figure 2 from a bilayer beam in the fully oxidized and reduced (neutral) states and in the intermediate straight position that was used as a reference. The beam appears to be thicker in the deflected states because it twisted slightly. (For clarification, “reduced” in this context means held at -1.0 V, determined experimentally to be sufficient to produce the maximum deflection during these cycles; the actual oxidation level is unknown. Likewise, “fully oxidized” means an applied voltage of +0.4 V.)

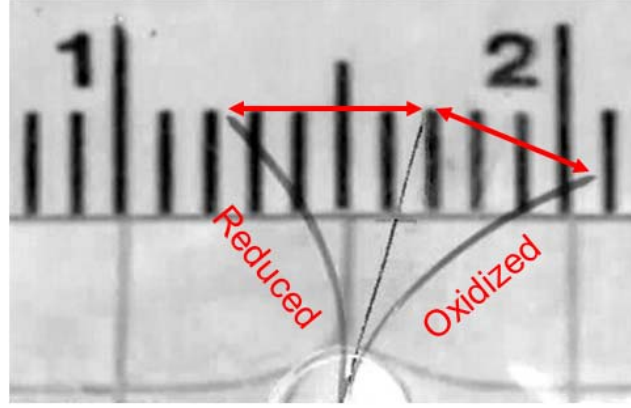


Figure 2. Three superimposed images of beam deflection upon reduction, oxidation, and transitioning midway (overhead view with the face of the beam perpendicular to the page). The ruler scale is in cm. The center position illustrates the zero curvature reference point that was used to determine tip deflections, and the arrows drawn over the image indicate the magnitude of the tip deflection.

Image processing was performed on still frames from the video to isolate the beam from the background (ImageJ software, NIH). An edge-detection algorithm written for this application (Matlab, Mathworks) was used to track the deflection δ of the tip of the beam. The recorded times from the video and the galvanostat were used to synchronize the cyclic voltammetry (CV) cycles with the deflection. The zero-curvature inflection points were obtained from the frames with the straightest beams. Beam curvature κ was calculated from measured tip deflections without assuming small deflections, as described in the Supporting Information.

$$(1) \quad \kappa = \frac{2\Delta x}{(L - \Delta y)^2 + \Delta x^2}$$

The actuation strain α_{PPy} was calculated from the curvature κ [33, 53, 54]:

$$(2) \quad \kappa = \frac{\alpha_{PPy}}{h_{sub}} \frac{6mn(1+m)}{1+4mn+6m^2n+4m^3n+m^4n^2}$$

where h_{sub} is the substrate thickness, m is the PPy to substrate thickness ratio (h_{PPy} / h_{sub}), and n is the ratio of the Young's moduli (E_{PPy} / E_{sub}). An effective E_{sub} was calculated from the combined substrate layers (see the Supporting Information). The Young's modulus of PPy(DBS) has been shown to change from 200 MPa in the reduced state to 450 MPa in the oxidized state [23]. Therefore, the oxidized state E_{PPy} was used to find the strain from the curved state (PPy side in) and the reduced state E_{PPy} was used to find the strain from the backwards-bending curvature. The two strains were summed to determine the effective actuation strain between the oxidized and reduced states.

2.4 Electrochemical break-in

The as-deposited PPy(DBS) is compact, and it typically takes several cycles for the structure to open fully to accommodate ion ingress [37, 55], particularly for thick films. Therefore, the bilayer beams were “primed” by performing ten cyclic voltammograms (CV cycles), ramping the voltage between +0.4 V and -1.0 V at 10 mV/s at room temperature (RT, ~22 °C) in 0.15 M NaDBS. The scan rate of 10 mV/s was chosen to enable observation of the shapes and positions of the oxidation and reduction peaks in the CV [29], and to compare the results to prior work.

2.5 Scanning electron microscopy and elemental analysis

After cycling, the polymer was taken to 0 V (oxidized) before switching off the voltage. Samples were rinsed in DI water and allowed to dry in air at room temperature for at least 24 hours. The final 5 mm section at the tip of the bilayer was cut off using a razor blade and adhered to a sample holder with double-sided copper/nickel adhesive tape. SEM images were obtained (Philips XL30ESEM, 5 kV) and the ions in the PPy were identified using energy dispersive x-ray analysis (Phoenix XEDS EDX, EDAX Inc.) with a 20 kV accelerating voltage. The spectra were normalized by the maximum intensity sulfur peak, and the resulting profiles were compared (Spectrum View v4.0, EDAX Inc.).

3 RESULTS AND DISCUSSION

3.1 Deflection during cyclic voltammetry in NaDBS at room temperature

The cycling behavior of PPy(DBS) in aqueous NaDBS at room temperature was used as a baseline because this polymer has previously been characterized in this electrolyte [23, 56]. Since the DBS⁻ is not exchanged, only the Na⁺ contributes to the volume change [36, 57], causing an expansion (and thus bilayer bending PPy-side out) during reduction as the hydrated Na⁺ enters the polymer and a contraction (bending PPy-side in) during oxidation as the hydrated Na⁺ leaves the polymer. (OH⁻ in the solution also enters and exits the polymer, but it does not contribute to actuation [58].)

Twelve bilayer devices were initially cycled ten times (cycles 1-10) in NaDBS at RT from +0.4 V to -1.0 V vs Ag/AgCl at 10 mV/s to bring them all to the same starting condition. (The samples were “primed”.) The NaDBS concentration was 0.15 M, matching the cation concentration in CSF. Sample-to-sample variation in the bending of these nominally identical samples is shown in the Supporting Information.

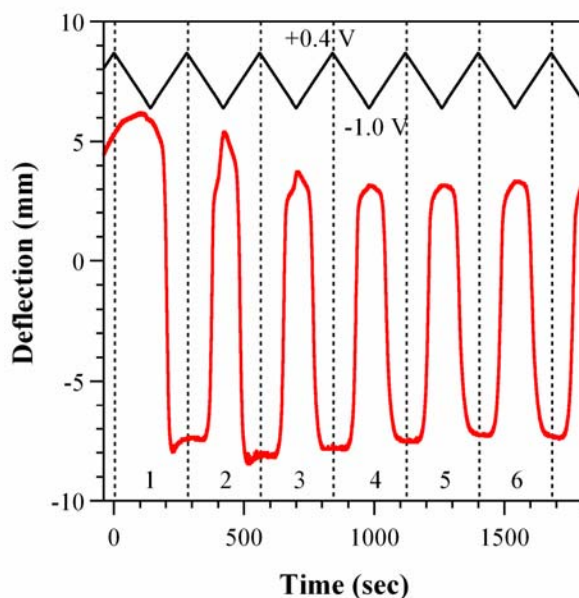


Figure 3. Deflection vs. time (lower red curve) during the first 6 cycles (numbered) of a bilayer in NaDBS at room temperature. The voltage was scanned at 10 mV/sec between +0.4 and -1.0 V vs Ag/AgCl, as illustrated at the top (black curve). Positive deflection indicates PPy expansion (bending PPy-side out), and negative deflection indicates PPy contraction (PPy-side in).

Figure 3 shows the deflection versus time of one of the bilayers during the initial cycling in NaDBS at RT. The samples began (at $t = -40$ sec) curved with the PPy side out (bending “backwards”). This curvature is not seen in thinner films of $1 \mu\text{m}$ [59], but is consistently observed in bilayers with thicker PPy films. During the initial increase in potential from 0 to +0.4 V (to the left of the first dashed vertical line), the deflection increased somewhat, indicating a small expansion of the PPy. The gradual increase in deflection continued upon scan reversal to the reduced state at -1.0 V ($t = 150$ sec). Such a lack of significant bilayer movement during the first reduction scan, despite the influx of Na^+ , is typical of PPy(DBS) [58, 60], which expands out-of-plane at this time [61]. Upon re-oxidation (going from -1.0 to +0.4 V), the PPy contracted strongly inplane as the Na^+ was expelled, reversing the direction of bending so that the PPy faced in (shown by negative numbers on the axis), passing through a point at which the bilayer was flat. Thereafter, the second reduction led to an expansion back to nearly the original position. The deflection versus time curves stabilized after the third or fourth cycle. This behavior is consistent with prior work, in terms of general behavior and the number of cycles required for “break in” (or priming or conditioning).

3.2 Cyclic voltammograms under four conditions

Immediately after the priming step, the samples were split into four groups of three samples each and cycled ten times (cycles 11-20) as before but in either (1) NaDBS at room temperature (NaDBS at RT), (2) NaDBS at body temperature (NaDBS at 37°C), (3) the physiological electrolyte at room temperature (aCSF at RT), or (4) the physiological electrolyte at body temperature (aCSF at 37°C).

The cyclic voltammograms (CVs) and the associated deflections during scan 19 in the four solutions are shown for representative samples in Figure 4. (Scan 20 concluded at 0 V, so to compare the deflection and charge consumed with scans ending at full oxidation (0.4 V), scans 9 and 19 were taken as representative of the steady state. The CVs for all 20 scans of all 12 samples are shown in the Supporting Information.)

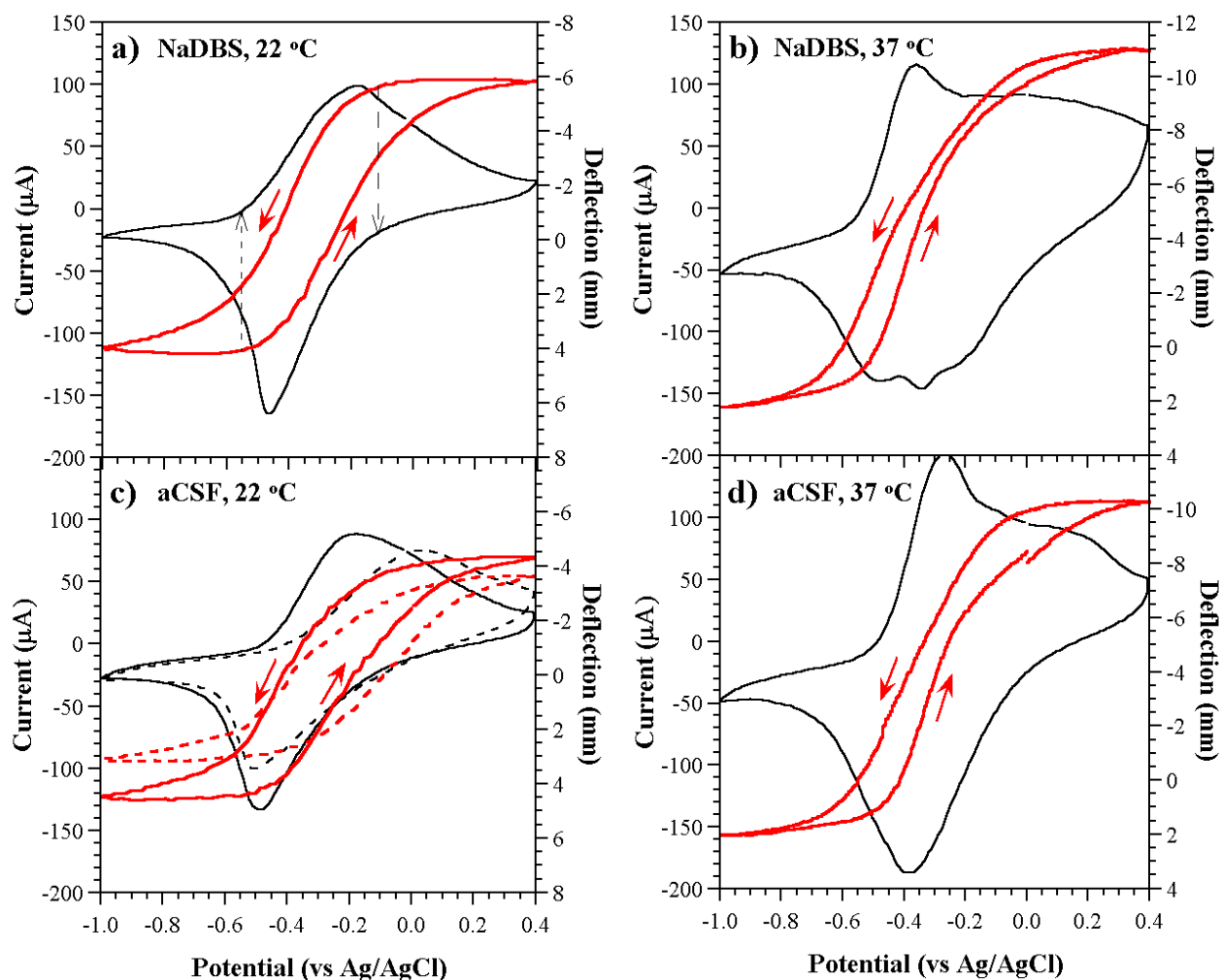


Figure 4. Current (black line) and displacement (thicker red line) as a function of potential during the 19th CV scan at 10 mV/s under four conditions. The direction of the scan for the displacement curves is indicated by arrows; note that this axis has been reversed to facilitate comparison with the current. The deflection axis is shifted in (b) and (d) relative to (a) and (c), but has the same amplitude (16 mm). The dashed lines in (c) show results from a second sample.

The CV for NaDBS at RT (Figure 4a, the control) was as expected from prior work [29], with a reduction peak near -0.45 V and an oxidation peak at -0.15 V with a shoulder visible near -0.35 V. Table 2 shows average values for the three samples in each group of the exchanged charge in both the priming step and, as ratios, in the subsequent cycling under the four conditions. (Values for all groups of samples during scans 9 and 19 are included in the Supporting Information.) Comparing

the average charge densities consumed by these samples during cycle 19 compared to cycle 9 (Table 2, data line 6), there was a 9% increase. Variations between samples were of similar magnitude, so we do not consider this 9% to be significant.

Table 2. Values of average actuation strain α , exchanged charge density, and strain-to-charge density in the 9th scan in NaDBS (12 samples) and average ratios of the 19th to the 9th scans under different cycling conditions (n = 3 unless otherwise noted).

Measurements	Values in NaDBS, Scan 9		Ratio of Scans 19/9			
			NaDBS		aCSF	
			RT	37C	RT	37C
α Reduction	0.37		1.09 ± 0.43	0.58 ± 0.09	0.86 ± 0.33	0.40 ± 0.28
α Oxidation	-0.36	%	0.93 ± 0.42	1.53 ± 0.18	0.93 ± 0.31	1.28 ± 0.22
α Total	0.73		1.02 ± 0.40	1.13 ± 0.09	0.89 ± 0.32	0.94 ± 0.19
Re Charge Density	-98±14*10 ⁶	C/m ³	1.11 ± 0.18	1.78 ± 0.42	1.02 ± 0.20	1.68 *
Ox Charge Density	79±11*10 ⁶		1.06 ± 0.21	1.56 ± 0.26	1.01 ± 0.19	1.71 *
Total Charge Density	178±24*10 ⁶		1.09 ± 0.18	1.66 ± 0.30	1.02 ± 0.23	1.70 *
Re α / Charge Density	38 ± 14 * 10 ⁻¹²	%/ (C/m ³)	0.99 ± 0.42	0.33 ± 0.09	0.84 ± 0.36	0.24 ± 0.17
Ox α / Charge Density	45 ± 14 * 10 ⁻¹²		0.87 ± 0.43	0.98 ± 0.20	0.92 ± 0.35	0.75 ± 0.13
Tot α / Charge Density	41 ± 14 * 10 ⁻¹²		0.94 ± 0.40	0.68 ± 0.13	0.87 ± 0.37	0.55 ± 0.11

(*) Denotes data from one sample.

At 37 °C, the CVs of the devices cycled in NaDBS changed significantly (Figure 4b). There was now a large oxidation peak at -0.35 V (the position at which the shoulder had been at RT), and a second broad oxidation peak appeared that was centered around +0.1 V; there was no clear peak at -0.15 V. In addition, two more reduction peaks appeared to the right of the peak at -0.45 V, at -0.35 V and -0.25 V. The area bounded by the CV was significantly larger: the exchanged charge density was 66% greater when cycling at 37 °C than at RT.

The CVs in aCSF at RT (Figure 4c) varied in their oxidation peak positions among the three samples, so two examples are shown. In general, the CVs were similar to those in NaDBS at RT, but the reduction peak was shifted slightly (30 mV) cathodically (i.e., to the left), and the oxidation peak was shifted anodically (to the right) in two cases but not the third. The total exchanged charge density was virtually the same as in NaDBS at RT.

Upon increasing the temperature in aCSF (Figure 4d), the changes in the oxidation current mirrored those in NaDBS at 37 °C (Figure 4b), and again the position of the large peak was shifted anodically relative to the one in NaDBS at 37 °C. The two satellite peaks during reduction were not present, however. (The CVs are overlaid for ease of comparison in the Supporting Information.) The total exchanged charge density again increased compared to aCSF at RT, by a similar factor (70%) as seen in NaDBS.

3.3 Actuation strains during CVs

Given the significant changes in the CVs, the important question was whether there were similar significant changes in actuation strain. In PPy(ClO₄) more exchanged charge is associated with

greater strain, until a degradation point [62, 63], but in PPy(DBS) currents can flow that are not associated with volume change [64]. Returning again to Figure 4a but this time examining the associated deflection, the contraction of the PPy (note the reversed right axis) began simultaneously with the onset of the oxidation current (shown by the dotted black arrow on the left), slowing down after the peak as the current dropped but continuing to +0.4 V. Expansion was also concurrent with the flow of charge during reduction (dashed black arrow) and continued all the way to -1.0 V.

As shown in Table 2 (data line 3, column 1), the average net strain (found using equation (1) from the displacements) in NaDBS at RT was only 0.7%, substantially less than the previously reported ~3% [23, 33, 35]. The reasons for this are unclear. The maximum voltages experienced during deposition were below +0.55 V vs. Ag/AgCl, so the PPy films were not over-oxidized. Samples were examined by SEM at cross-sections midway through the beams, and beams demonstrating delamination were excluded from the analysis. However, partial delamination cannot be ruled out; this would have reduced the curvature since only part of the PPy film would have contributed to actuation. PPy films in contact with a conductor along their entire area have been shown to produce a force density six-fold greater than isolated films [12]. There is some evidence for delamination in the CVs shown in the Supporting Information, in which the currents steadily decrease in each cycle and the peak positions shift.

The ratio of the strain to the charge density was on the order of $0.4 \cdot 10^{-10} \text{ \%}/(\text{C}/\text{m}^3)$. Previous values (at RT) were 3x as high for PPy(tetraethylammonium hexafluorophosphate) at $1.2\text{-}1.4 \cdot 10^{-10} \text{ \%}/(\text{C}/\text{m}^3)$ (electro-polymerized, cycled in propylene carbonate) [65, 66] and two orders of magnitude higher for PPy(sodium benzenesulfonate) at $30 \cdot 10^{-10} \text{ \%}/(\text{C}/\text{m}^3)$ (films purchased from BASF, cycled in acetonitrile) [67, 68].

As it should have, the average net strain remained effectively unchanged from cycle 9 to cycle 19 in NaDBS at RT (2% increase - Table 2, line 3, column 2), although there was a small shift in the position; this is discussed in more detail below. The average consumed charge increased by 9%, leading to a somewhat smaller strain to charge ratio (6% decrease). These variations provide context for interpreting the magnitude of changes under the other cycling conditions, since nominally the conditions were unchanged here from the priming conditions: variations of this size should not be considered meaningful, but due to experimental variations.

The overall actuation behavior in aCSF at RT (Figure 4c) could be described in the same way as in NaDBS. The actuation strain decreased somewhat (-11% relative to scan 9 for this group of devices in NaDBS) while the current density was unchanged, resulting in a correspondingly smaller strain to charge ratio. Most importantly, there was no reversal in the direction of movement despite the anions in this solution, and no significant loss of strain over time due to the divalent cations.

Despite the substantial changes in the CVs when the temperature was raised to 37 °C in NaDBS, the actuation strain varied relatively little from that at RT, increasing by a factor of 1.13 on average. (The particular sample in Figure 4b increased much more; the other two pairs of curves are shown in the Supporting Information.) Because of the large increase in the consumed charge (66%), the strain to charge ratio dropped to 0.68 of the value at RT. At elevated temperatures, the actuators were thus less efficient in converting electrical energy to mechanical energy. There was also a large shift of several mm in the positions of the deflections (equilibrium bending angle), as seen by comparing the

values of the deflection axis limits in Figure 4a and c. This behavior is further discussed below and needs to be taken into account in designing actuators for use at body temperature. The new oxidation peak at +0.1/0.2 V did not contribute significantly to the volume change, and again there was no reversal in the direction of movement even though the oxidation process corresponding to that peak has previously been correlated with anion ingress [22]. It is not clear why there is a new oxidation peak unassociated with bilayer motion at 37 °C, and this should be the topic of future investigation.

In aCSF, although 67% more charge was exchanged at 37 °C than at 22 °C, the net strain only increased by 6% on average, reducing the strain to charge density. These results mirrored those in heated NaDBS. Again, there was a shift in the average bending angle.

These experiments show that these actuators behave substantially the same under physiological settings as in NaDBS, with the movement monotonically increasing/decreasing with voltage at these scan rates. Monotonic behavior is important for actuator control, and was a welcome surprise because the presence of Cl⁻ anions has previously been reported to result in tip deflection in one direction as the cations exit followed shortly thereafter by deflection in the opposite direction as anions enter [22, 69].

3.4 Maximum deflection during CVs

As mentioned previously, there were shifts in the average bending angle for the four experimental groups relative to the baseline primed condition. Figure 5 shows the maximum deflections during oxidation and reduction of one representative bilayer in each group of three under each of the four conditions over all twenty CV cycles. (The behavior of the three beams in each set was similar, as demonstrated in the Supporting Information.)

As discussed for Figure 3, during the first several cycles the magnitude of the deflection in both directions decreased, but then it then stabilized. The curves for bilayers that continued cycling in NaDBS at RT (open blue circles) leveled out to show no further change over time. Those cycled in aCSF at RT (filled blue circles) experienced an immediate small decrease in total peak-to-peak deflection (8% on average), and thereafter the deflections remained constant (leveling off at a 10% average decrease).

The changes with temperature were larger, as also reflected in Figure 4. Samples cycled at 37 °C (red triangular points) in both aCSF (filled symbols) and NaDBS (open symbols), showed a contraction of the PPy, with both positive and negative deflections shifting relative to the previous cycles; this likely reflects a structural change in the polymer. Deflection during oxidation was more strongly shifted, resulting in an overall *net increase* in the range of motion by ~2.5 mm. These results are consistent with previously observed increased strain at higher temperatures [41, 42].

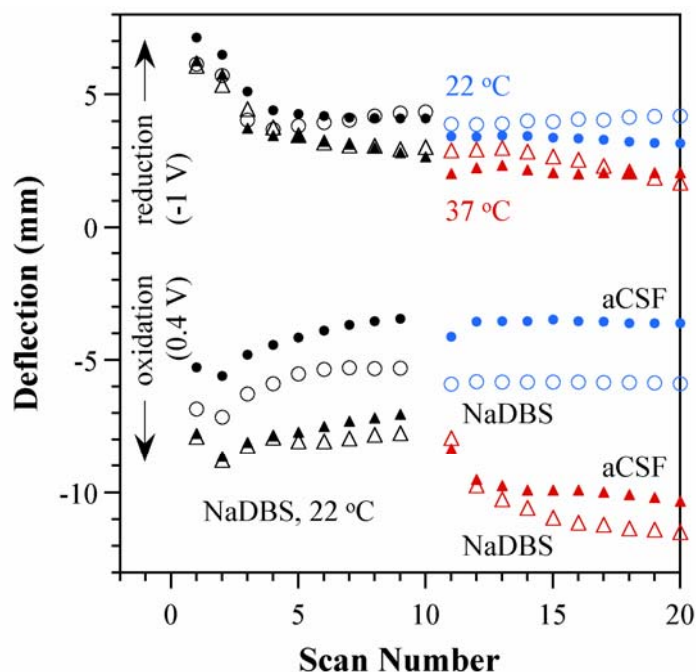


Figure 5. a) Maximum deflection of representative bilayers during oxidation and reduction during cyclic voltammetry as a function of cycle number. Black symbols: actuation in NaDBS at room temperature (all samples during cycles 1-10). Filled symbols: actuation in aCSF during cycles 11-20; open symbols: actuation in NaDBS; red triangle symbols, actuation at 37 °C during cycles 11-20; blue circle symbols, actuation at room temperature.

3.5 Elemental analysis

To shed light on the actuation changes noted above, energy-dispersive x-ray spectroscopy (EDX) was performed. There were small variations among the three samples under each condition, so the spectra were averaged. Figure 6 shows the average EDX spectra from the samples that had been cycled in NaDBS at RT and from those cycled in aCSF at 37 °C. The spectra were normalized to the sulfur (S) peak; results were virtually identical using the carbon (C) peak. A nickel peak (at 8.26 keV, not shown) indicated that the beam penetrated the entire thickness of the sample.

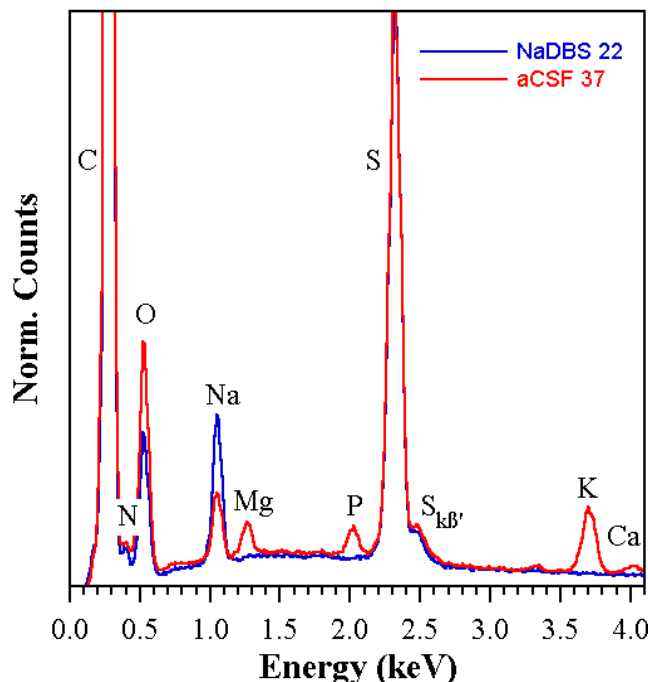


Figure 6. EDX spectra of samples cycled in NaDBS at 22 °C and in aCSF at 37 °C, normalized to the S peak.

The sample cycled in NaDBS contained carbon (C) from the PPy and the DBS, nitrogen (N) from the PPy, and oxygen (O) and sulfur (S) from the DBS. It also contained sodium (Na) from the electrolyte. Recall that the sample was taken to the oxidized state before removing it from the electrochemical cell, so this reflects Na^+ that is deeply trapped in the film (presumably with the associated water). A small $S_{KB'}$ shift peak, an indication of the S oxidation state, is also visible to the right of the S peak [70]. The sample cycled in aCSF contained the same species, but it also showed magnesium (Mg), calcium (Ca), potassium (K), phosphorous (P), and additional oxygen (O) (the latter two from the PO_4) incorporated into the polymer during cycling. There was no Cl in these samples (k_α 2.622, k_β 2.815 eV) (although we found trace amounts in two samples in a previous study [71]).

EDX is not quantitative without comparison to a reference sample with a similar composition. Furthermore, the areas under EDX peaks for *different* species cannot be used to obtain relative concentrations, so these spectra can only be used to compare relative amounts of the same element. The area under the Na peak for the sample cycled in aCSF was 68% of the size for the sample cycled in NaDBS (72% if normalizing to the C peak instead of the S peak), so we can hypothesize that a third less Na^+ was exchanged during cycling in aCSF. (This conclusion assumes that if there was any loss of Na^+ during sample rinsing and drying, it occurred in the same proportion in both solutions.)

The difference in compensating charge was made up by the other cations. Given their low concentration in aCSF (Table 1), we can conclude that the PPy affinity for K^+ , Ca^{2+} , and Mg^{2+} is higher than for Na^+ . We have previously shown that K^+ produces smaller strains than Na^+ [44] (K^+

has a smaller hydration shell), so the decrease in deflection in aCSF may be partly due to its exchange. As mentioned above, divalent cations interact more strongly with the PPy chains and thus have greater difficulty exiting the polymer, resulting in less polymer expansion, so one might speculate that the decrease in deflection in aCSF may also be related to that.

In addition, it has been shown that in solutions containing small anions, that they are also exchanged during cycling, despite the presence of the immobile DBS⁻ [22, 69]. Interestingly, essentially no Cl⁻ was found in the sample, despite a concentration in aCSF nearly as high as that of Na⁺. Instead, the oxygen peak in the aCSF samples was 60% larger (75% larger if normalizing to the C peak), and with each PO₄ carrying 4 oxygens and each DBS carrying three, we can tentatively conclude that one PO₄ is entering for each two DBSs. This is a surprisingly large amount, given its minute concentration in aCSF (~0.5% that of Cl⁻). We have previously seen differences in the affinity of PPy(DBS) to different cations, but this difference to the two anions is particularly large. Prior work with PPy(PPS) tested in sodium phosphate buffer showed an anodic peak [46], but in our CVs there were no observable peaks associated with this exchange (compare Figure 4a and c). (It is not the peak at +0.1 V, since that also appeared in NaDBS.) The PO₄ molecule is in the form of PO₄³⁻ at high pH, but becomes increasingly protonated as the pH is lowered until it becomes H₃PO₄ in acidic media. (In CSF, which has a pH of 7.3, the proportions would be expected to be 61% HPO₄²⁻ and 39% H₂PO₄⁻.) The local pH at the surface of the polymer is unknown, but the local pH is known to be affected by cycling [58, 72]. Nevertheless, the molecule is an anion, rather than a cation. Again, half a PO₄ per DBS is an enormous amount, and one might have expected that to cause a noticeable reversal in the deflection (Figure 4), particularly given that its reported hydrated radius is nearly as large as that of Na⁺ (Table 1), but it did not. The prior study with PPy(PPS) in sodium phosphate buffer also showed no volume change [46]. It is possible that much slower scans may show actuation strain, or that PO₄ has such a small hydration shell in the PPy that it is mechanically “invisible.” Further studies would be required to understand this.

4 CONCLUSIONS

The bending of bilayer bending beams actuated using PPy(DBS) was characterized under physiological conditions similar to those found in the brain. These conditions were simulated by employing aCSF at 37 °C, which contains a mixture of cations, including two divalent cations, as well as a couple of small anions. The roles of both temperature and of the mix of ions were ascertained by making use of a control solution containing only a single type of cation and no mobile anions (NaDBS) and by comparing bending at 22 °C and 37 °C. As discussed above, divalent ions have been shown to ionically crosslink charged polymers, resulting in difficulties in exchanging these ions and producing smaller strains, posing the concern that device performance would degrade in the aCSF. Another concern arose from the presence of the small anions, which in prior work had been shown to produce a reversal of motion, complicating positional control over devices (as well as reducing net strain).

The actuation strain in aCSF at 22 °C was almost 90% of that in NaDBS, and furthermore it remained monotonic. The exchanged charge was also virtually the same. Thus, neither the divalent cations nor the small anions had a significant negative impact, even though elemental analysis revealed that all the cationic components of aCSF were present in substantial amounts in the PPy after cycling, in addition to a large amount of HPO_4^{2-} and/or H_2PO_4^- (one per 2 DBSs). Interestingly, the ion content in the film did not reflect the solution composition, which had at least 200 times more chlorine than phosphate and 25 times more sodium than all the other cations combined. Temperature exerted a more significant change in behavior. The net strain increased somewhat at 37 °C in both solutions, and the average bending angle shifted noticeably. These effects will need to be taken into account when designing devices for use in the body. The cyclic voltammograms acquired additional peaks and substantially more charge was exchanged, resulting in a lower efficiency in converting electrical to mechanical work. Nevertheless, it is clear that PPy(DBS) can indeed be used for neural interface and neural probe applications.

ACKNOWLEDGMENTS

This work was supported by the Center for Neural Communication Technology is a P41 Resource Center funded by the National Institute of Biomedical Imaging and Bioengineering (NIBIB, P41 EB002030) and supported by the National Institutes of Health (NIH).

SUPPORTING INFORMATION

Supporting information includes cyclic voltammetry and deflection of all twelve bilayers under all four conditions, peak to peak deflections for the samples, variation among samples, deflection upon voltage stepping, transient effects upon voltage stepping, ramping voltage to attenuate initial transient effects, calculation of curvature and actuation strain from deflection measurements, and cross-sectional images showing delamination in some devices.

REFERENCES

- [1] E. Smela, "Conjugated polymer actuators for biomedical applications," *Adv. Mater.*, 15, 481-494, 2003.
- [2] C. Immerstrand, K. Holmgren-Peterson, K. E. Magnusson, E. Jager, M. Krogh, M. Skoglund, A. Selbing, and O. Inganäs, "Conjugated-polymer micro- and milliactuators for biological applications," *MRS Bull.*, 27, 461-464, 2002.
- [3] P. M. George, A. W. Lyckman, D. A. LaVan, A. Hegde, Y. Leung, R. Avasare, C. Testa, P. M. Alexander, R. Langer, and M. Sur, "Fabrication and biocompatibility of polypyrrole implants suitable for neural prosthetics," *Biomaterials*, 26, 3511-3519, 2005.
- [4] R. A. Green, N. H. Lovell, G. G. Wallace, and L. A. Poole-Warren, "Conducting polymers for neural interfaces: Challenges in developing an effective long-term implant," *Biomaterials*, 29, 3393-3399, 2008.
- [5] K. K. C. Lee, N. R. Munce, T. Shoa, L. G. Charron, G. A. Wright, J. D. Madden, and V. X. D. Yang, "Fabrication and characterization of laser-micromachined polypyrrole-based artificial muscle actuated catheters," *Sens. Act. A*, 153, 230-236, 2009.
- [6] E. W. H. Jager, E. Smela, and O. Inganäs, "Microfabricating conjugated polymer actuators," *Science*, 290, 1540-1545, 2000.
- [7] C. E. Schmidt, V. R. Shastri, J. P. Vacanti, and R. Langer, "Stimulation of neurite outgrowth using an electrically conducting polymer," *Proc. Natl. Acad. Sci.*, 94, 8948-8953, 1997.
- [8] R. L. Williams and P. J. Doherty, "A preliminary assessment of poly(pyrrole) in nerve guide studies," *J. Mater. Sci. Mater. Med.*, 5, 429-433, 1994.
- [9] X. D. Wang, X. S. Gu, C. W. Yuan, S. J. Chen, P. Y. Zhang, T. Y. Zhang, J. Yao, F. Chen, and G. Chen, "Evaluation of biocompatibility of polypyrrole in vitro and in vivo," *J. Biomed. Mater. Res. A*, 68A, 411-422, 2004.
- [10] D. D. Ateh, H. A. Navsaria, and P. Vadgama, "Polypyrrole-based conducting polymers and interactions with biological tissues," *J. R. Soc. Interface*, 3, 741-752, 2006.
- [11] B. Shapiro and E. Smela, "Bending actuators with maximum curvature and force and zero interfacial stress," *J. Intel. Mat. Syst. Str.*, 18, 181-186, 2007.
- [12] A. S. Hutchison, T. W. Lewis, S. E. Moulton, G. M. Spinks, and G. G. Wallace, "Development of polypyrrole-based electromechanical actuators," *Synth. Met.*, 113, 121-127, 2000.
- [13] L. Bay, K. West, and S. Skaarup, "Pentanol as co-surfactant in polypyrrole actuators," *Polymer*, 43, 3527-3532, 2002.

- [14] E. Smela, "Microfabrication of PPy microactuators and other conjugated polymer devices," *J. Micromech. Microeng.*, 9, 1-18, 1999.
- [15] Y. Liu, Q. Gan, S. Baig, and E. Smela, "Improving PPy adhesion by surface roughening," *J. Phys. Chem. C*, 111, 11329-11338, 2007.
- [16] J. G. Cham, E. A. Branchaud, Z. Nenadic, B. Greger, R. A. Andersen, and J. W. Burdick, "Semi-chronic motorized microdrive and control algorithm for autonomously isolating and maintaining optimal extracellular action potentials," *J. Neurophysiol.*, 93, 570-579, 2005.
- [17] D. V. Palanker, A. Vankov, P. Huie, and S. A. Baccus, "Design of a high-resolution optoelectronic retinal prosthesis." *J. Neural Eng.*, 2, S105-S120, 2005.
- [18] B. S. Wilson and M. F. Dorman, "Cochlear implants: A remarkable past and a brilliant future," *Hear. Res.*, 242, 3-21, 2008.
- [19] J. A. Saint-Cyr, T. Hoque, L. C. M. Pereira, J. O. Dostrovsky, W. D. Hutchison, D. J. Mikulis, A. Abosch, E. Sime, A. E. Lang, and A. M. Lozano, "Localization of clinically effective stimulating electrodes in the human subthalamic nucleus on magnetic resonance imaging," *J. Neurosurg.*, 97, 1152-1166, 2002.
- [20] E. D. Daneshvar, D. R. Kipke, and E. Smela, "Navigating conjugated polymer actuated neural probes in a brain phantom," *Proc. SPIE Smart Struct. Mater. (EAPAD)*, San Diego, vol. 8340, 09.1-09.12, edited by Y. Bar-Cohen (March 12-15, 2012).
- [21] M. J. M. Jafeen, M. A. Careem, and S. Skaarup, "Speed and strain of polypyrrole actuators: dependence on cation hydration number," *Ionics*, 16, 1-6, 2010.
- [22] S. Skaarup, L. Bay, K. Vidanapathirana, S. Thybo, P. Tofte, and K. West, "Simultaneous anion and cation mobility in polypyrrole," *Solid State Ionics*, 159, 143-147, 2003.
- [23] L. Bay, N. Mogensen, S. Skaarup, P. Sommer-Larsen, M. Jorgensen, and K. West, "Polypyrrole doped with alkyl benzenesulfonates," *Macromolecules*, 35, 9345-9351, 2002.
- [24] A. G. MacDiarmid, "Synthetic metals: a novel role for organic polymers," *Synth. Met.*, 125, 11-22, 2001.
- [25] A. F. Diaz and J. Bargon, "Electrochemical synthesis of conducting polymers " in Handbook of Conducting Polymers, T. A. Skotheim, Ed., (Dekker, New York, 1986).
- [26] T. Shoa, T. Mirfakhrai, and J. D. W. Madden, "Electro-stiffening in polypyrrole films: Dependence of Young's modulus on oxidation state, load and frequency," *Synth. Met.*, 160, 1280-1286, 2010.

- [27] J. Kielland, "Individual activity coefficients of ions in aqueous solutions," *J. Am. Chem. Soc.*, 59, 1675-1678, 1937.
- [28] M. A. Careem, K. P. Vidanapathirana, S. Skaarup, and K. West, "Dependence of force produced by polypyrrole-based artificial muscles on ionic species involved," *Solid State Ionics*, 175, 725-728, 2004.
- [29] M. A. Careem, Y. Velmurugu, S. Skaarup, and K. West, "A voltammetry study on the diffusion of counter ions in polypyrrole films," *J. Power Sources*, 159, 210-214, 2006.
- [30] T. Shimizu and A. Minakata, "Effect of divalent cations on the volume of a maleic acid copolymer gel examined by incorporating lysozyme," *Eur. Polym. J.*, 38, 1113-1120, 2002.
- [31] R. John and G. G. Wallace, "Doping-dedoping of polypyrrole: a study using current-measuring and resistance-measuring techniques," *J. Electroanal. Chem.*, 354, 145-160, 1993.
- [32] M. R. Gandhi, P. Murray, G. M. Spinks, and G. G. Wallace, "Mechanism of electromechanical actuation in polypyrrole," *Synth. Met.*, 73, 247-256, 1995.
- [33] M. Christophersen, B. Shapiro, and E. Smela, "Characterization and modeling of PPy bilayer microactuators - Part 1. Curvature," *Sens. Act. B*, 115, 596-609, 2006.
- [34] E. Smela and N. Gadegaard, "Surprising volume change in PPy(DBS): An atomic force microscopy study," *Adv. Mater.*, 11, 953-957, 1999.
- [35] Q. B. Pei and O. Inganäs, "Electrochemical applications of the bending beam method: 1. Mass-transport and volume changes in polypyrrole during redox," *J. Phys. Chem.*, 96, 10507-10514, 1992.
- [36] S. Skaarup, K. West, L. M. W. K. Gunaratne, K. P. Vidanapathirana, and M. A. Careem, "Determination of ionic carriers in polypyrrole," *Solid State Ionics*, 136, 577-582, 2000.
- [37] H. Yang and J. Kwak, "Mass transport investigated with the electrochemical and electrogravimetric impedance techniques. 2. Anion and water transport in PMPy and PPy films," *J. Phys. Chem. B*, 101, 4656-4661, 1997.
- [38] Q. B. Pei and O. Inganäs, "Electrochemical applications of the bending beam method; a novel way to study ion-transport in electroactive polymers," *Solid State Ionics*, 60, 161-166, 1993.
- [39] B. Gaihre, S. Ashraf, G. M. Spinks, P. C. Innis, and G. G. Wallace, "Comparative displacement study of bilayer actuators comprising of conducting polymers, fabricated from polypyrrole, poly(3,4-ethylenedioxythiophene) or poly(3,4-propylenedioxythiophene)," *Sens. Act. A*, 193, 48-53, 2013.

- [40] N. Vandesteeg, P. G. Madden, J. D. Madden, P. A. Anquetil, and I. W. Hunter, "Synthesis and characterization of EDOT-based conducting polymer actuators," *Proc. SPIE Smart Struct. Mater. (EAPAD)*, San Diego, vol. 5051, 349-356, edited by Y. Bar-Cohen (March 2-6, 2003).
- [41] M. Christophersen and E. Smela, "Polypyrrole/gold bilayer microactuators: Response time and temperature effects," *Proc. SPIE Smart Struct. Mater. (EAPAD)*, San Diego, vol. 6168, (February 27 - March 2, 2006).
- [42] S. Fanning. , "*Characterization of polypyrrole/gold bilayers for micro-valve design*," PhD. dissertation, University of Maryland, College Park, MD, 2005.
- [43] J. D. Madden, D. Rinderknecht, P. A. Anquetil, and I. W. Hunter, "Creep and cycle life in polypyrrole actuators," *Sens. Act. A*, 133, 210-217, 2007.
- [44] X. Z. Wang and E. Smela, "Cycling conjugated polymers with different cations," *Proc. SPIE Smart Struct. Mater. (EAPAD)*, San Diego, vol. 6168, (February 27-March 2, 2006).
- [45] S. Maw, E. Smela, K. Yoshida, and R. B. Stein, "Effects of monomer and electrolyte concentrations on actuation of PPy(DBS) bilayers," *Synthetic Metals*, 155, 18-26, 2005.
- [46] S. S. Pandey, W. Takashima, and K. Kaneto, "Conserved electrochemomechanical activities of polypyrrole film in complex buffer media," *Sens. Act. B*, 102, 142-147, 2004.
- [47] W. Takashima, S. S. Pandey, and K. Kaneto, "Cyclic voltammetric and electrochemomechanical characteristics of freestanding polypyrrole films in diluted media," *Thin Solid Films*, 438, 339-345, 2003.
- [48] E. C. McNay and R. S. Sherwin, "From artificial cerebro-spinal fluid (aCSF) to artificial extracellular fluid (aECF): microdialysis perfusate composition effects on in vivo brain ECF glucose measurements," *J. Neurosci. Methods*, 132, 35-43, 2004.
- [49] I. S. Kass, A. A. Bendo, A. E. Abramowicz, and J. E. Cottrell, "Methods for studying the effect of anesthetics on anoxic damage in the rat hippocampal slice," *J. Neurosci. Methods*, 28, 77-82, 1989.
- [50] S. Maw, E. Smela, K. Yoshida, P. Sommer-Larsen, and R. B. Stein, "The effects of varying deposition current density on bending behaviour in PPy(DBS)-actuated bending beams," *Sens. Act. A*, 89, 175-184, 2001.
- [51] S. Skaarup, K. West, B. Zachaustriansen, M. A. Careem, and G. K. R. Senadeera, "Electrolyte and ion memory effects in highly conjugated polypyrrole," *Solid State Ionics*, 72, 108-114, 1994.

- [52] K. West, T. Jacobsen, B. Zachaustriensen, M. A. Careem, and S. Skaarup, "Electrochemical synthesis of polypyrrole - Influence of current-density on structure," *Synth. Met.*, 55, 1412-1417, 1993.
- [53] S. P. Timoshenko, "Analysis of bi-metal thermostats," *J. Opt. Soc. Am.*, 11, 233-255, 1925.
- [54] J. M. Gere and S. P. Timoshenko, Mechanics of Materials, 4th ed. (PWS-KENT Publishing Company, Boston, 1997).
- [55] H. Yang and J. Kwak, "Mass transport investigated with the electrochemical and electrogravimetric impedance techniques. 1. Water transport in PPy/CuPTS films," *J. Phys. Chem. B*, 101, 774-781, 1997.
- [56] B. J. West, T. F. Otero, B. Shapiro, and E. Smela, "Chronoamperometric study of conformational relaxation in PPy(DBS)," *J. Phys. Chem. B*, 113, 1277-1293, 2009.
- [57] M. A. Depaoli, R. C. D. Peres, S. Panero, and B. Scrosati, "Properties of electrochemically synthesized polymer electrodes .10. Study of polypyrrole dodecylbenzenesulfonate," *Electrochim. Acta.*, 37, 1173-1182, 1992.
- [58] S. Shimoda and E. Smela, "The effect of pH on polymerization and volume change in PPy(DBS)," *Electrochim. Acta.*, 44, 219-238, 1998.
- [59] E. Smela, M. Kallenbach, and J. Holdenried, "Electrochemically driven polypyrrole bilayers for moving and positioning bulk micromachined silicon plates," *J. Microelectromech. Syst.*, 8, 373-383, 1999.
- [60] P. Chiarelli, A. Della Santa, D. De Rossi, and A. Mazzoldi, "Actuation properties of electrochemically driven polypyrrole freestanding films," *J. Intell. Mater. Syst. Struct.*, 6, 32-37, 1995.
- [61] E. Smela and N. Gadegaard, "Volume change in polypyrrole studied by atomic force microscopy," *J. Phys. Chem. B*, 105, 9395-9405, 2001.
- [62] T. F. Otero, J. J. López Cascales, and G. Vázquez Arenas, "Mechanical characterization of free-standing polypyrrole film," *Mat. Sci. Eng. C*, 27, 18-22, 2007.
- [63] T. F. Otero, M. Márquez, and I. J. Suárez, "Polypyrrole: Diffusion coefficients and degradation by overoxidation," *J. Phys. Chem. B*, 108, 15429-15433, 2004.
- [64] X. Z. Wang and E. Smela, "Color and volume change in PPy(DBS)," *J. Phys. Chem. C*, 113, 359-368, 2009.

- [65] J. D. W. Madden, P. G. A. Madden, and I. W. Hunter, "Polypyrrole actuators: modeling and performance," *Proc. SPIE Smart Struct. Mater. (EAPAD)*, Newport Beach, vol. 4329, 72-83, edited by Y. Bar-Cohen (March 5-8, 2001).
- [66] P. A. Anquetil, D. Rinderknecht, N. A. Vandesteeg, J. D. Madden, and I. W. Hunter, "Large strain actuation in polypyrrole actuators," *Proc. SPIE Smart Struct. Mater. (EAPAD)*, San Diego, vol. 5385, 380-387, edited by Y. Bar-Cohen (March 15-18, 2004).
- [67] A. Della Santa, D. De Rossi, and A. Mazzoldi, "Characterization and modelling of a conducting polymer muscle-like linear actuator," *Smart Mater. Struct.*, 6, 23-34, 1997.
- [68] A. Della Santa, D. De Rossi, and A. Mazzoldi, "Performance and work capacity of a polypyrrole conducting polymer linear actuator," *Synth. Met.*, 90, 93-100, 1997.
- [69] K. P. Vidanapathirana, M. A. Careem, S. Skaarup, and K. West, "Ion movement in polypyrrole/dodecylbenzenesulphonate films in aqueous and non-aqueous electrolytes," *Solid State Ionics*, 154, 331-335, 2002.
- [70] A. J. Ramponi and J. M. Jaklevic, "The application of X-ray emission spectra to the identification of particulate sulfur compounds in ambient air," Technical Report, Lawrence Berkeley Lab., California Univ., Berkeley., LBL-7284, December 1978.
- [71] E. D. Daneshvar, E. Smela, and D. R. Kipke, "Mechanical characterization of conducting polymer actuated neural probes under physiological settings," *Proc. SPIE Smart Struct. Mater. (EAPAD)*, San Diego, vol. 7642, 1T.1-1T.10, edited by Y. Bar-Cohen (March 7-11, 2010).
- [72] H. Shinohara, J. Kojima, and M. Aizawa, "Electrically controlled ion transfer and pH change near a conducting polymer-coated electrode," *J. Electroanal. Chem.*, 266, 297-308, 1989.
- [73] X. Z. Wang, B. Shapiro, and E. Smela, "Visualizing ion currents in conjugated polymers," *Adv. Mater.*, 16, 1605-1609, 2004.
- [74] Q. B. Pei and O. Inganäs, "Electrochemical applications of the bending beam method: 2. Electroshrinking and slow relaxation in polypyrrole," *J. Phys. Chem.*, 97, 6034-6041, 1993.
- [75] T. F. Otero and J. M. Garcia de Otazo, "Polypyrrole oxidation: Kinetic coefficients, activation energy and conformational energy," *Synth. Met.*, 159, 681-688, 2009.
- [76] W. Lu, E. Smela, P. Adams, G. Zuccarello, and B. R. Mattes, "Development of solid-in-hollow electrochemical linear actuators using highly conductive polyaniline," *Chem. Mater.*, 16, 1615-1621, 2004.
- [77] W. C. Young, Roark's formulas for stress & strain, 6th ed. (McGraw-Hill, Inc., 1989).

- [78] *Specialty Coating Systems SCS Parylene Properties*, 2010, (Accessed: 11/8/2011), Available: <http://www.scscoatings.com/docs/coatspec.pdf>.
- [79] J. P. Seymour and D. R. Kipke, "Fabrication of polymer neural probes with Sub-cellular features for reduced tissue encapsulation," *Conf. Proc. IEEE Eng. Med. Biol. Soc.*, New York, vol. 1, (August 30-September 3, 2006).
- [80] C. Y. Shih, T. A. Harder, and Y. C. Tai, "Yield strength of thin-film parylene-C," *Microsyst. Technol.*, 10, 407-411, 2004.
- [81] V. K. Pamula, A. Jog, and R. B. Fair, "Mechanical property measurement of thin-film gold using thermally actuated bimetallic cantilever beams," *Nanotech.*, 1, 410-413, 2001.
- [82] J. Lintymer, N. Martin, J. M. Chappe, J. Takadoum, and P. Delobelle, "Modeling of Young's modulus, hardness and stiffness of chromium zigzag multilayers sputter deposited," *Thin Solid Films*, 503, 177-189, 2006.
- [83] K. E. Petersen and C. R. Guarnieri, "Young's modulus measurements of thin films using micromechanics," *J. Appl. Phys.*, 50, 6761-6766, 1979.
- [84] M. Benslimane, P. Gravesen, K. West, S. Skaarup, and P. Sommer-Larsen, "Performance of polymer based actuators: The three-layer model," *Proc. SPIE Smart Struct. Mater. (EAPAD)*, Newport Beach, vol. 3669, 87-97, edited by Y. Bar-Cohen (March 1-4, 1999).

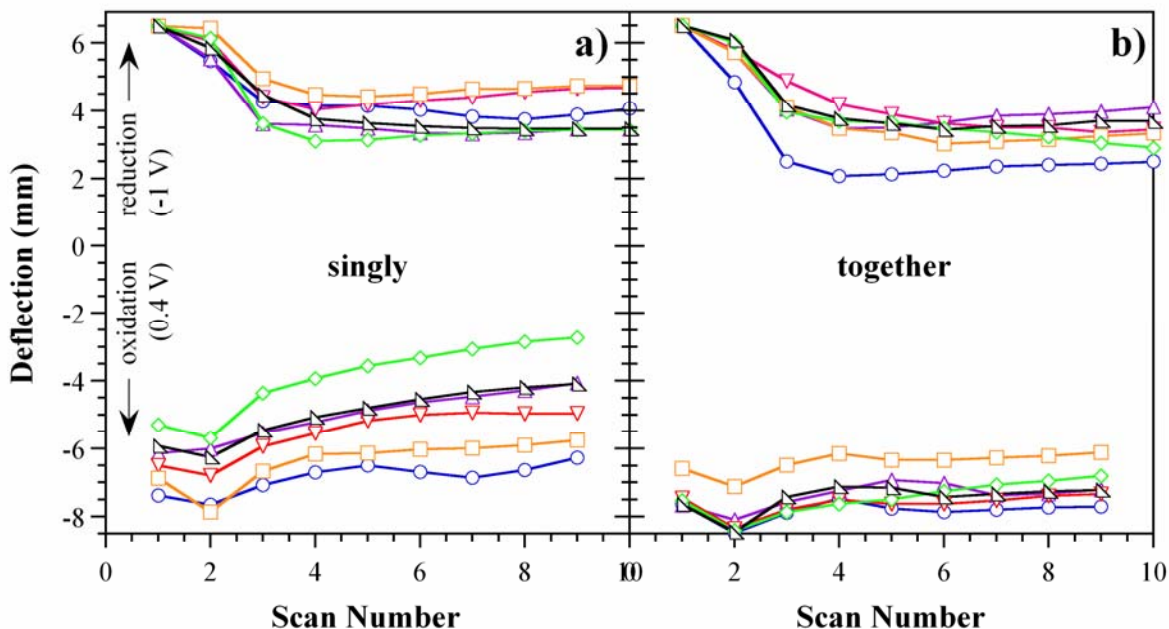
Supporting Information
for
Characterization of Conjugated Polymer Actuation
Under Cerebral Physiological Conditions

by

Eugene Dariush Daneshvar and Elisabeth Smela

S1. Variation among samples

In order to explore the extent of sample-to-sample variation under nominally identical electro-deposition and cycling conditions, six samples (the ones in Section 3.1 that were subsequently cycled at room temperature) that had been polymerized one at a time on the same day were compared with six samples (the ones in Section 3.1 that were later cycled at 37 °C) that had been polymerized simultaneously on another day. The same current density was used in all cases (1 mA/cm²).



Sup. Figure 1. Maximum deflection during oxidation and reduction in NaDBS at 22 °C as a function of cycle number. a) Six bilayers on which the PPy(DBS) was polymerized separately (one bilayer at a time). b) Six bilayers on which the PPy(DBS) was polymerized simultaneously.

Sup. Figure 1 shows the variation in maximum deflections for both sets of samples during the first 10 cycles in room temperature NaDBS. The initial deflections in the reduced state varied, with an average of 6.5 mm and a standard deviation of 0.6 mm. In order to facilitate comparison, all the

deflection data in Sup. Figure 1 were shifted so that the starting reduction position was the same, 6.5 mm.

The (shifted) average deflection during reduction in scan 10 was $4.0 \text{ mm} \pm 0.6 \text{ mm}$ for the films deposited separately and $3.3 \text{ mm} \pm 0.6 \text{ mm}$ for the PPy deposited simultaneously. The second set drifted somewhat further from the starting position, on average. The *variation* in the final reduced positions was the same $\pm 0.6 \text{ mm}$ for all twelve beams, however.

During oxidation the bilayers made together deflected more than those made individually and showed less variation in the oxidized-state starting positions: in scan 1 the average was $-6.3 \text{ mm} \pm 0.7 \text{ mm}$, compared with $-7.4 \text{ mm} \pm 0.4 \text{ mm}$ for the bilayers made together. The variation among bilayer tip positions increased by cycling: at scan 9, the average was $-4.6 \text{ mm} \pm 1.3 \text{ mm}$ for the individually-polymerized beams and for the beams polymerized together it was $-7.1 \text{ mm} \pm 0.6 \text{ mm}$.

These data indicate that there are differences among beams made on the same day, even if they are all made together, and that there is even greater variation if they are made one at a time. Nevertheless, the behavior was broadly similar for all the bilayers, showing a decrease in deflection within the first 4 cycles in both the PPy-side-out and PPy-side-in directions but stabilizing thereafter.

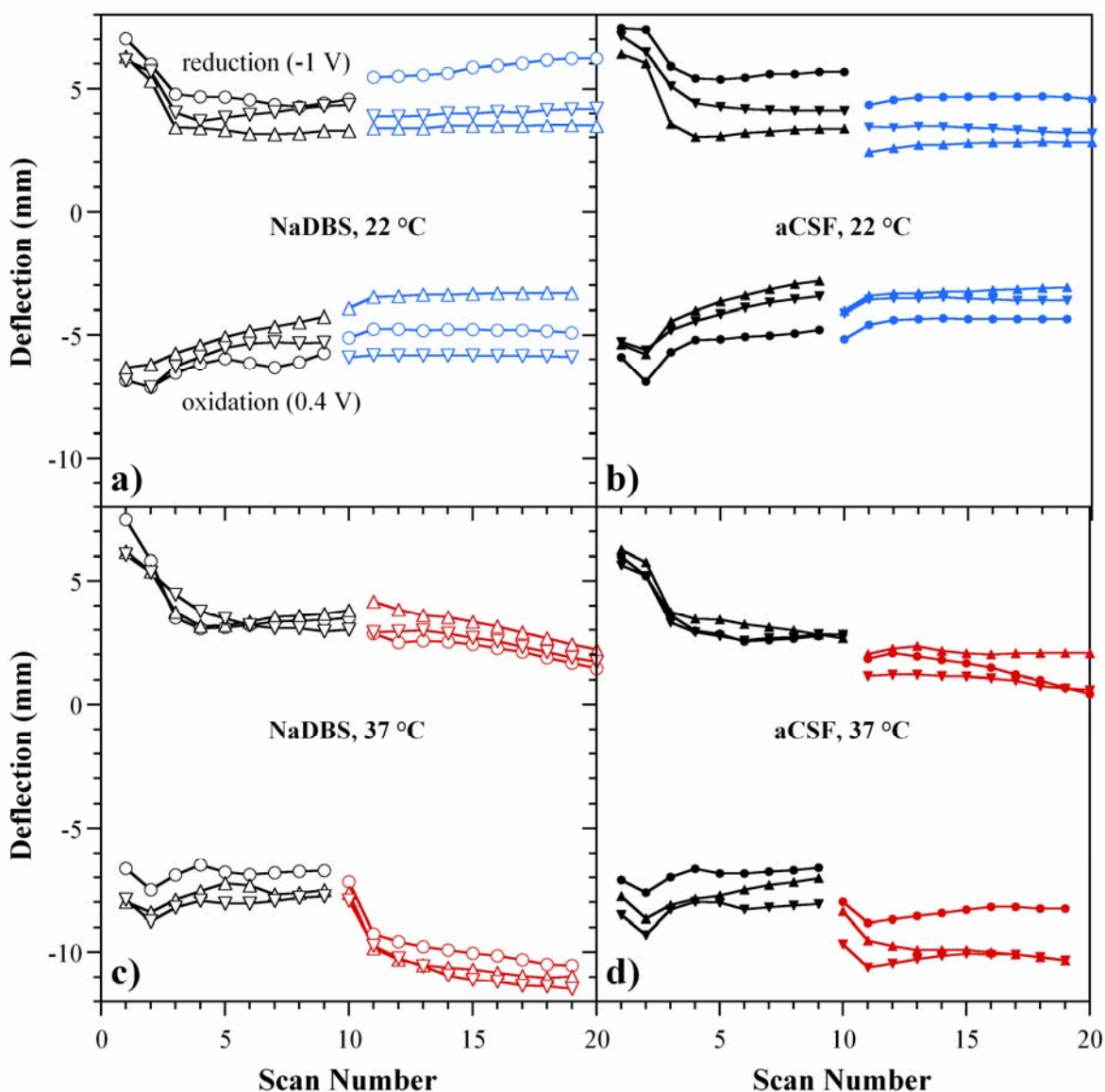
S2. Deflection of all twelve bilayers under all four conditions

The deflections of all the bilayers are shown in Sup. Figure 2. The samples used in the main text, Figure 5, were: NaDBS, 22 °C: ▼ (sample 2), aCSF, 22 °C: ▼ (sample 2), NaDBS, 37 °C: ▼ (sample 2), aCSF, 37 °C: ▲ (sample 3).

Sup. Table 1. Peak to peak deflections for the samples in Figure 5 of the main text.

Peak-to-Peak Deflection (mm)				
	NaDBS RT	NaDBS 37 °C	aCSF RT	aCSF 37 °C
Scan 9	9.61	10.70	7.56	9.84
Scan 19	10.03	13.27	6.80	12.26
Deflection Difference from Scan 19 to 9 (mm)				
Scan 19-9	0.42	2.56	-0.76	2.42
Peak-to-Peak Deflection Ratio (Scan 19/9)				
Scan 19/9	1.04	1.24	0.90	1.25

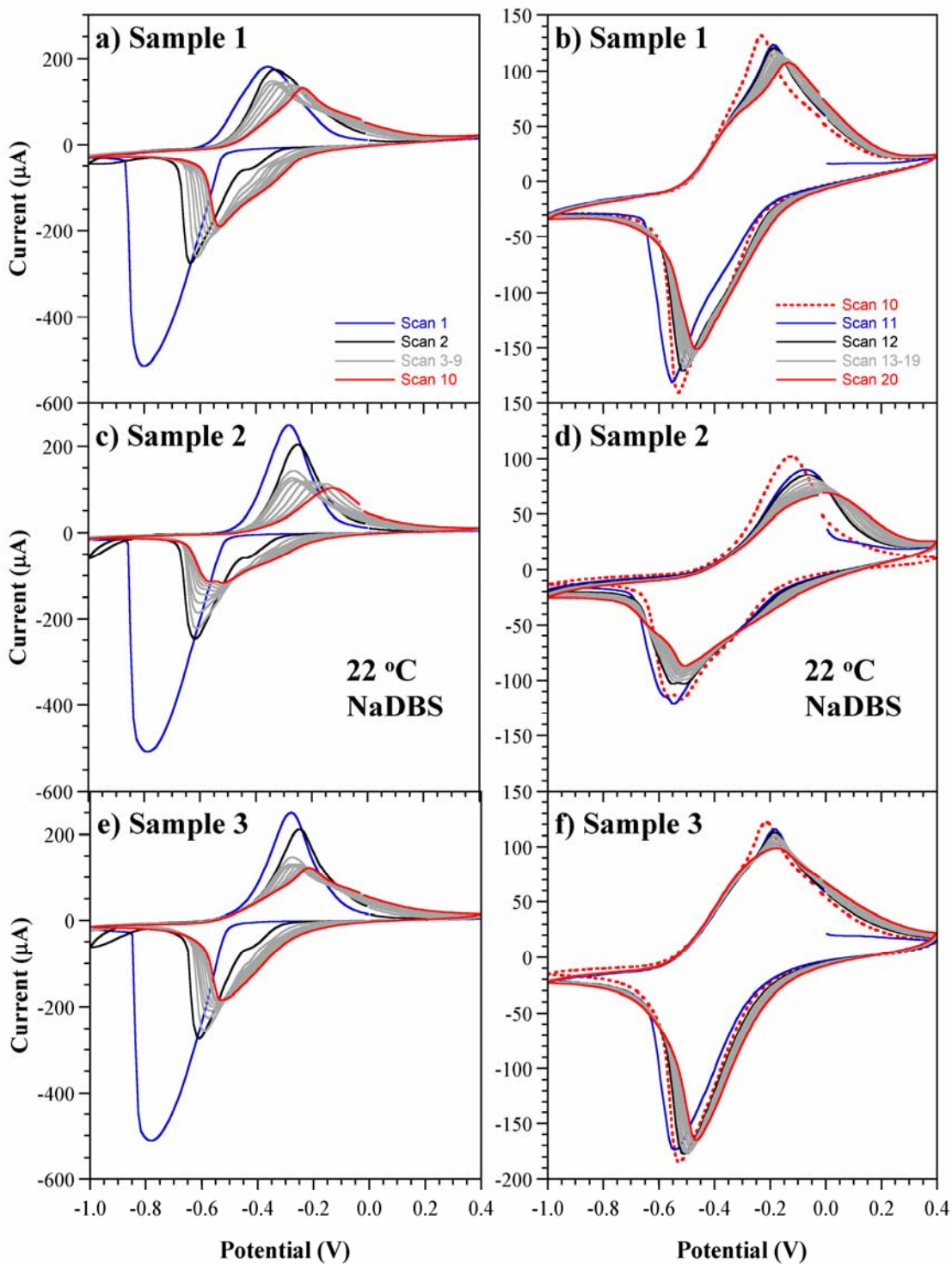
As shown in Figure 2 of the main text, during each CV scan the bilayer beam would deflect to a proximal position relative to the straight position during reduction and oxidation. Sup. Table 1 shows the net deflections in scans 9 and 19 for the samples shown in Figure 5 of the main text. In addition, the differences in displacements between scans 19 and 9 as well as their ratios are also given.



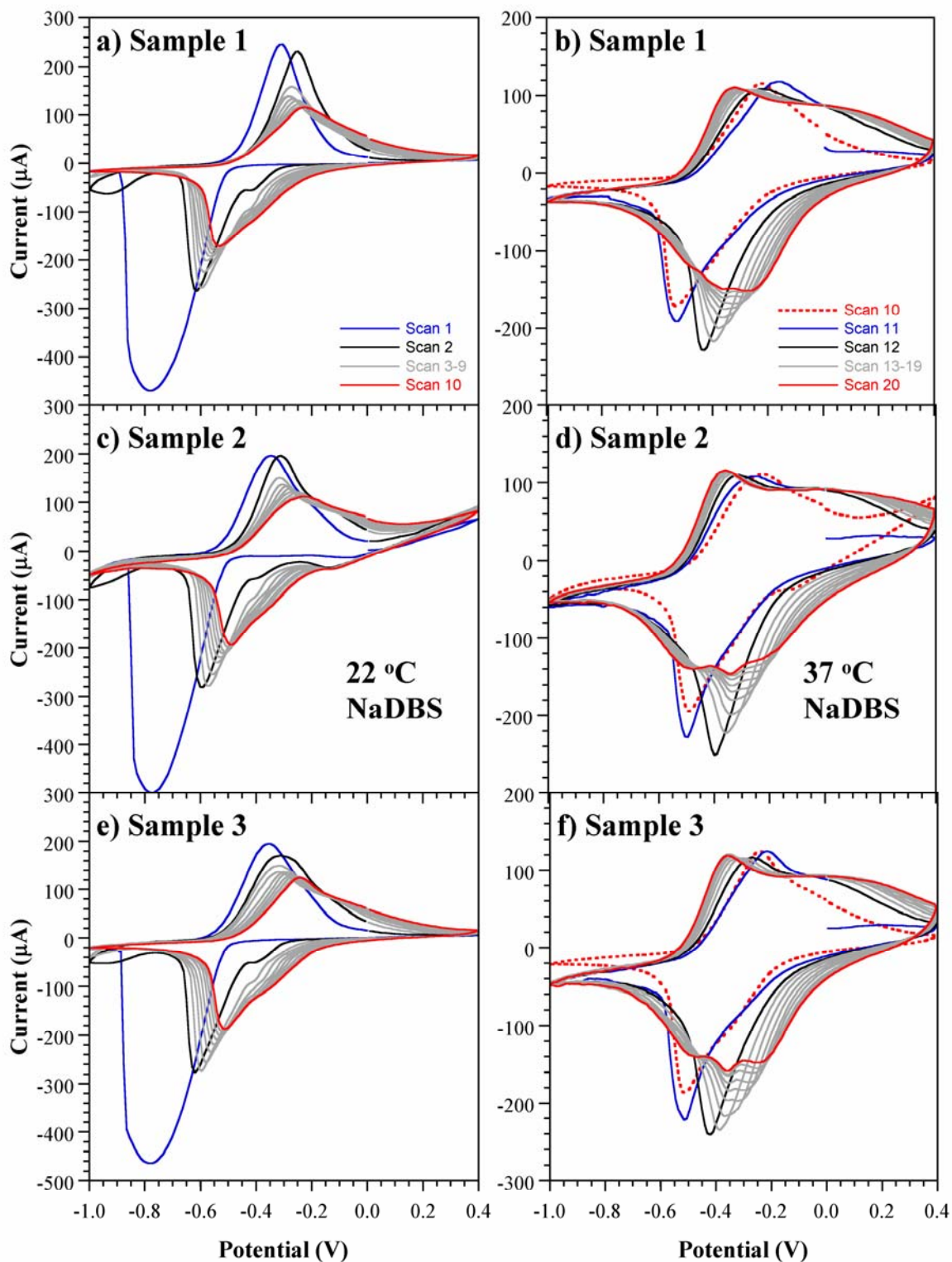
Sup. Figure 2. The maximum deflections during cyclic voltammetry of all twelve samples, cycled in NaDBS at 22 °C for the first 10 cycles, then in the medium and at the temperature indicated. (For correlation with Sup. Figure 3-Sup. Figure 6, circles = sample 1, up-pointing triangles = sample 2, and down-pointing triangles = sample 3.)

S3. Cyclic voltammetry of bilayers under the four conditions

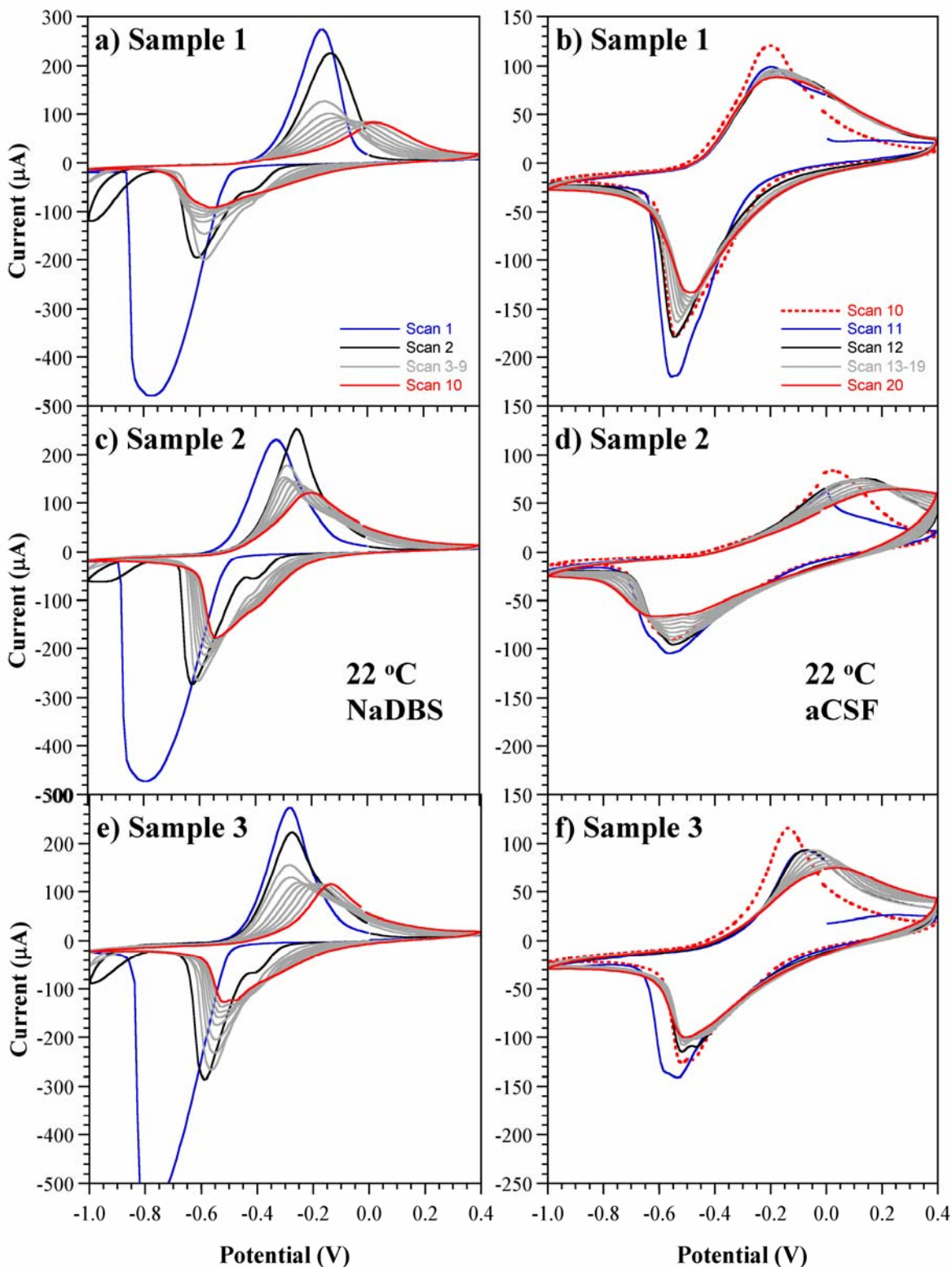
Figure 4 of the main text shows current-voltage relationships of representative samples in each of the four solutions. To illustrate the variability, the cyclic voltammograms (CVs) of all three samples in each of the four solutions are shown in Sup. Figure 3-Sup. Figure 6. PPy(DBS) was galvanostatically (constant current) polymerized to a thickness of $11.3 \pm 0.8 \mu\text{m}$. The scan rate was 10 mV/s, and the reference electrode was Ag/AgCl.



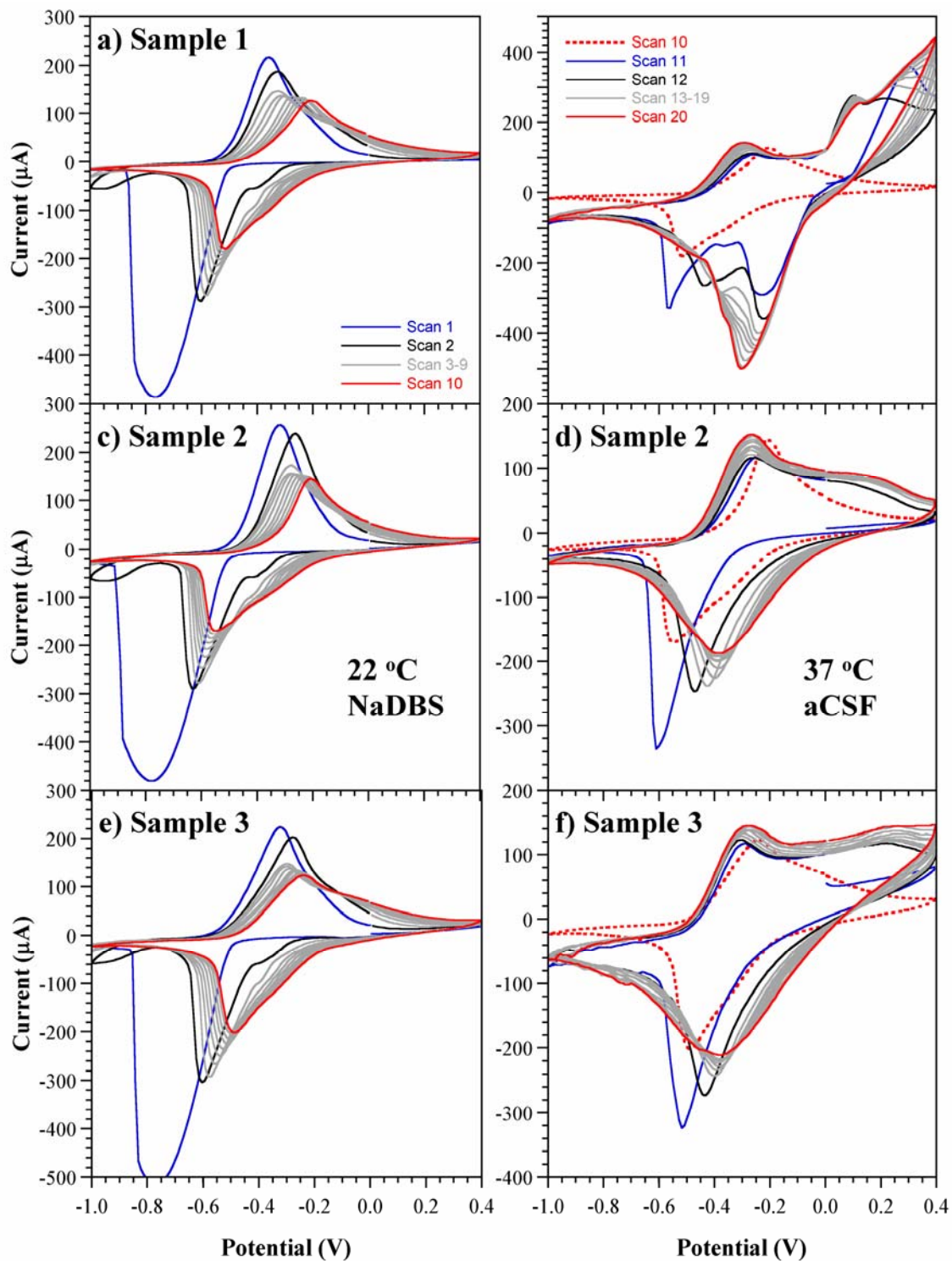
Sup. Figure 3. Cyclic voltammograms of three samples cycled in NaDBS at 22 °C for (left) the first 10 scans and then (right) the second 10 scans. To facilitate comparison, since the scales on the left and the right differ, scan 10 is repeated. Sample 3 was used in the main text.



Sup. Figure 4. Cyclic voltammograms of three samples cycled in NaDBS at (left) 22 °C for the first 10 scans and then (right) at 37 °C for the second 10 scans. Sample 2 was used in the main text.



Sup. Figure 5. Cyclic voltammograms of three samples cycled (left) in NaDBS at 22 °C for the first 10 scans and then (right) in aCSF at 22 °C for the second 10 scans. Sample 3 was used in the main text.

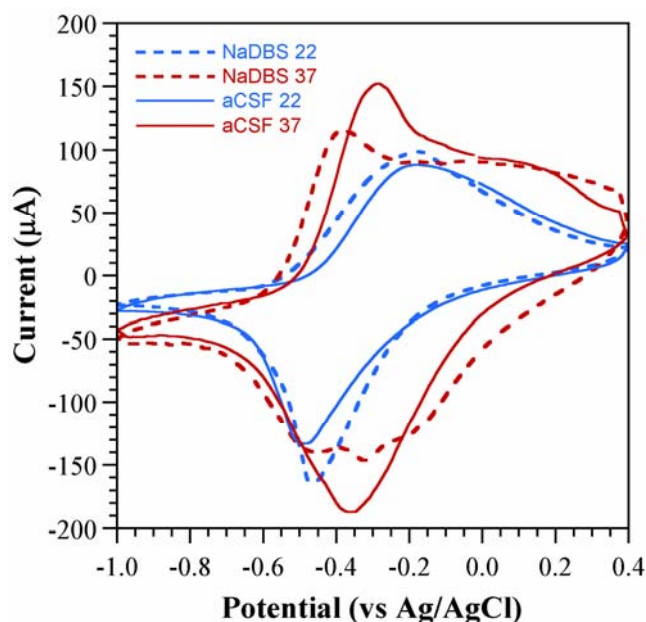


Sup. Figure 6. Cyclic voltammograms of three samples cycled (left) in NaDBS at 22 °C for the first 10 scans and then (right) in aCSF at 37 °C for the second 10 scans. Note that the vertical scale for (b) is almost twice that for (d) and (f). Sample 2 was used in the main text.

The expected large current is seen during the very first reduction scan in NaDBS [61]. Thereafter, the reduction peak shifts anodically (to the right) and decreases in height. The second scan shows a small current at -1 V that is not seen in any of the other scans. The oxidation peak shifts anodically and also decreases in size with scan number. The CVs have not completely stabilized after the first 10 scans. In Sup. Figure 3, the cycling continues in the same NaDBS solution, after the samples were removed from the cell and placed back into it. The anodic shifts and reductions in current magnitude continue. It is possible that an irreversible change is occurring, such as delamination. Sample 3 in Sup. Figure 3f is an exception, since the CVs more or less stabilize; this sample also has the highest currents, or exchanged charge, supporting the hypothesis that the others may be delaminating.

As noted above, the samples later cycled at room temperature (Sup. Figure 3 and Sup. Figure 5) were polymerized individually, while those later cycled at 37 °C (Sup. Figure 4 and Sup. Figure 6) were all polymerized together. The CVs of the former showed somewhat greater variability upon cycling in NaDBS than did the latter, but the basic behavior was the same.

Sup. Figure 7 overlays the current-voltage relationships in the four solutions in scan 19 for the samples of Figure 4 in the main text.

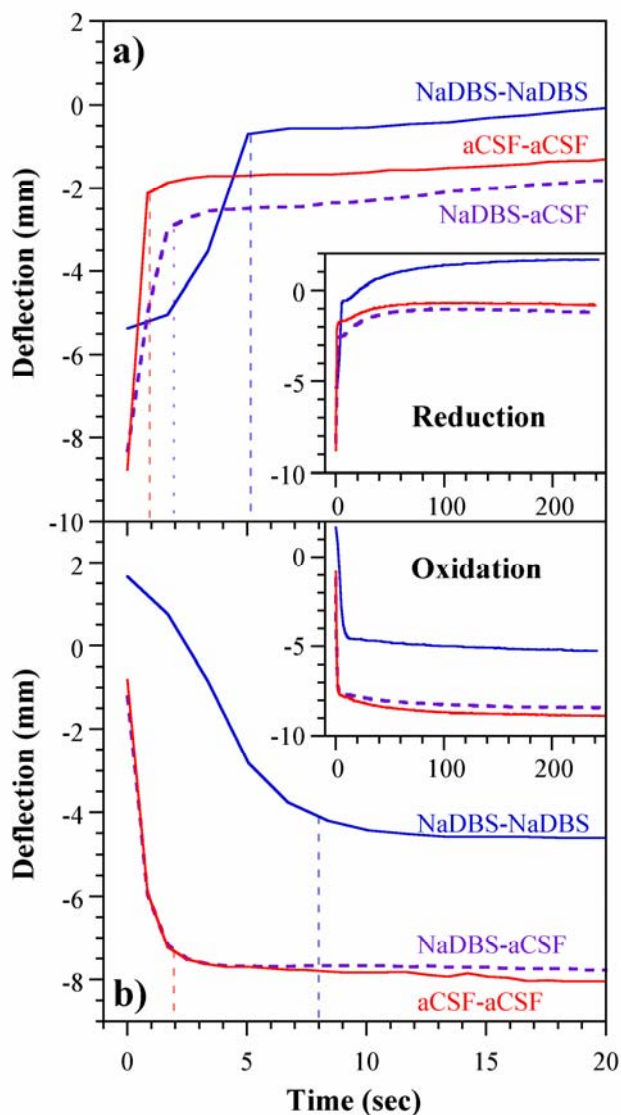


Sup. Figure 7. Typical cyclic voltammograms in the four solutions.

S4. Deflection upon voltage stepping

During slow potential scanning the deflection is limited by the scan rate, but under a voltage step the speed is determined by the rate-limiting oxidation or reduction process, typically mass transport of the solvated ions within the polymer [73]. To ascertain the speed of the actuators, voltage stepping was carried out. Three new samples were primed by performing ten CVs at 25 mV/s; two in NaDBS

at RT and one in aCSF at RT. Next, the samples were stepped ten times between 0.4 V and -1.0 V using a voltage square wave, holding each potential for 240 seconds. One was stepped in NaDBS at RT (NaDBS-NaDBS) and two in aCSF at 37 °C (NaDBS-aCSF & aCSF-aCSF). The tip deflections from the video and the current data were synchronized and segmented into reduction and oxidation partitions. The deflections from the final cycle are shown in Sup. Figure 8. Curve fitting was accomplished using Matlab, and rise and fall time constants were obtained.



Sup. Figure 8. Preliminary data for 3 samples (one per group). Deflection during the 10th step between 0.4 V and -1.0 V either in NaDBS at RT or in aCSF at 37 °C after prior electrochemical cycling in one of these two solutions at RT. NaDBS-NaDBS indicates priming in NaDBS followed by stepping in NaDBS.

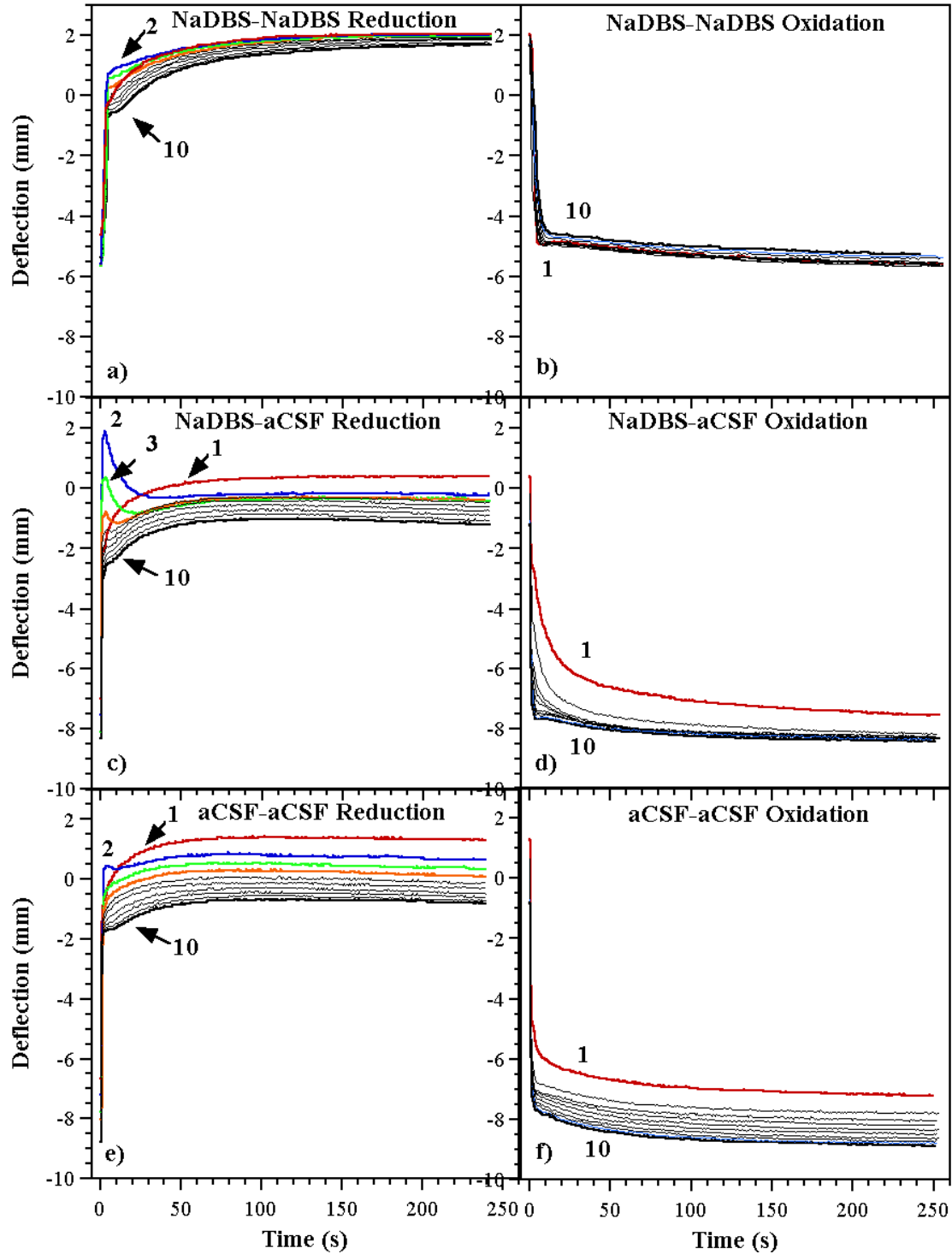
Tip deflections comprised an initial fast movement that took on the order of seconds (indicated by the dashed vertical lines) followed by a slower movement that took place on the order of hundreds of

seconds (shown in the inset). The two bilayers that were stepped in 37 °C aCSF moved more quickly during the first few seconds than the one in 22 °C NaDBS. The fast component, which would be the one used in actual applications, was approximately 5 seconds for reduction and 8 seconds for oxidation in 22 °C NaDBS, while it was 1-2 seconds for reduction and 2 seconds for oxidation in 37 °C aCSF, about 4 times faster. The increase in speed with temperature is fortunate for applications in the body.

Over longer times, the deflections gradually increased somewhat further. This is in the opposite direction as observed for salt draining in PPy(DBS) [74], instead suggesting a continued slow uptake of mass during reduction and loss of mass during oxidation, indicating a very slow-moving species or slow polymer chain motions [75].

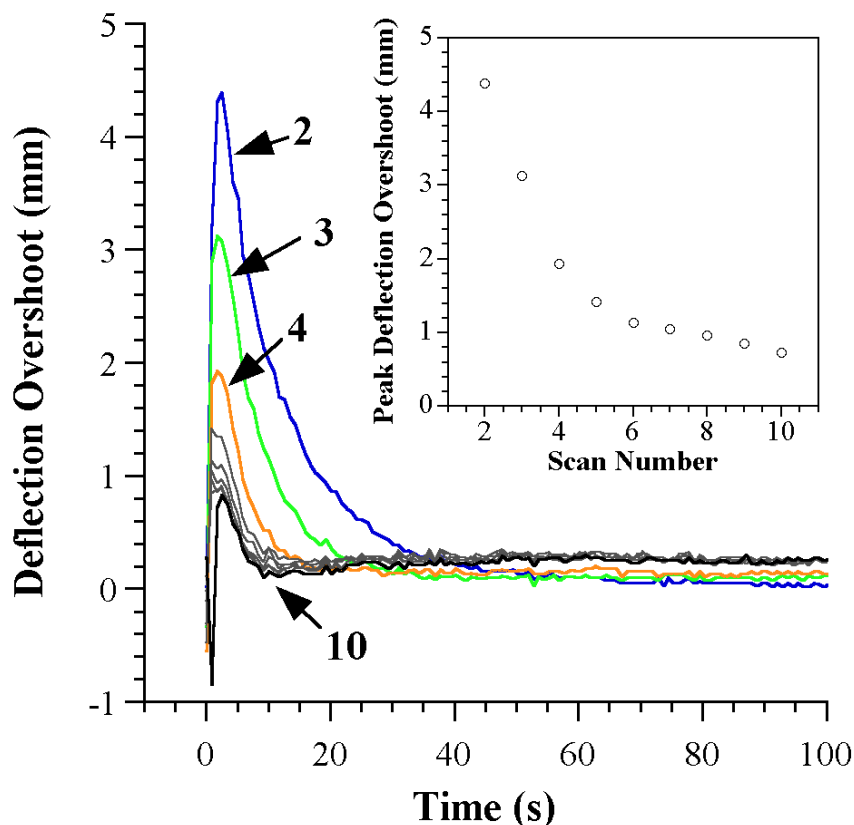
S5. Transient effects upon voltage stepping

The data in Sup. Figure 8 are for the 10th step in the second electrolyte. All 10 tip deflections in each electrolyte are shown in Sup. Figure 9. With each step, the final deflections under all three conditions, during both oxidation and reduction, shifted downward on the y axis, from positive displacements toward (more) negative ones. The shifts were larger in aCSF at 37 °C than they were in NaDBS at RT. For the NaDBS-aCSF (Sup. Figure 9c) condition, there were noticeable overshoots during reduction in which the deflection changed direction. Interestingly, the overshoot peak was not present during the first reduction step; instead, it was maximal in the second step and persisted until the fifth. A small overshoot was also seen in the second step upon raising the temperature from 22 °C to 37 °C in aCSF.



Sup. Figure 9. Preliminary data for 3 samples. Step responses of ten consecutive oxidation and reduction cycles, overlaid, in either NaDBS at RT or aCSF at 37 °C. Samples “NaDBS-aCSF” and “aCSF-aCSF” were stepped in 37 °C aCSF after priming in NaDBS at RT or aCSF at RT, respectively.

The transient deflection peaks during reduction of the NaDBS-aCSF sample were extracted from the deflection profile by subtracting scan 1 from subsequent scans and considering the “deflection overshoot” as the distance relative to scan 1’s steady state value. The resultant peaks indicate the differences in the initial response and are shown in Sup. Figure 10. Despite the fact that the tip reached a steady final value, the overshoot peak reappeared in the next scan, although its magnitude decayed in each subsequent step. Even after ten scans there was a residual 0.8 mm overshoot that decayed over 5 sec. This transient peak was not found in the NaDBS-NaDBS sample, and it was less prominent in the aCSF sample primed in aCSF.



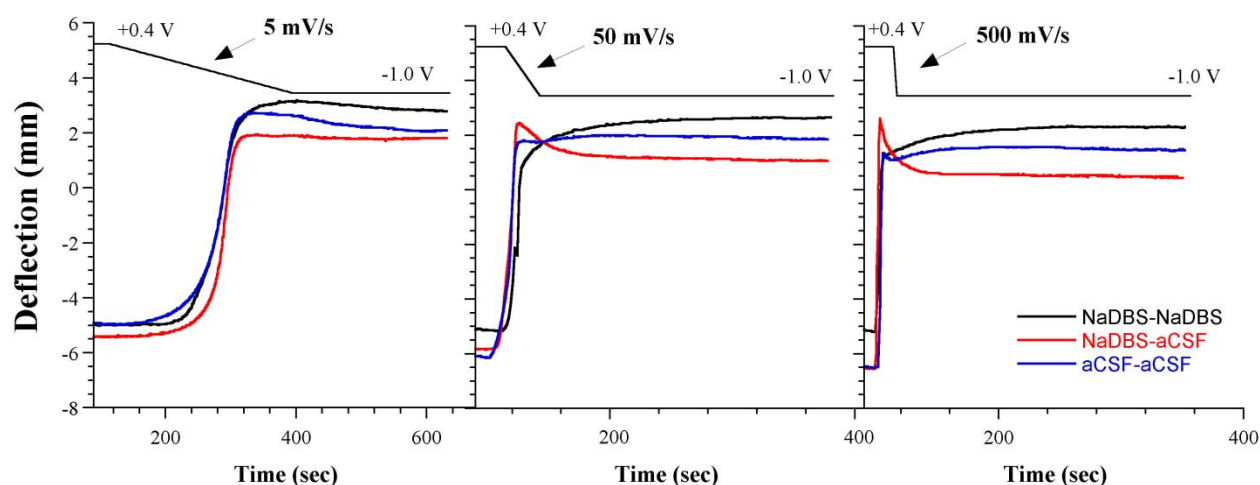
Sup. Figure 10. Preliminary data for 3 samples. Transient deflection peaks during reduction for scans 2-10 relative to scan 1 for the sample primed in NaDBS at RT and cycled in aCSF at 37 °C (NaDBS-aCSF, Sup. Figure 9c). Deflection overshoot is the difference of each scan relative to the steady state value of scan 1 (at 100 s). The peak deflection overshoots for scans 2-10 are plotted in the inset.

Reversals in beam motion have been seen when motion of one species in one direction is followed by motion of another species of the opposite charge in the opposite direction, with the time lag due to differences in mobility (and thus transport speeds) due to e.g. ion sizes [22, 40, 69, 76]. It is also known that the ions in conjugated polymers can be completely exchanged upon cycling in different electrolytes, and this was also shown for our PPy(DBS) system by the EDX spectra in Figure 6. The reduction in the amplitude of the overshoot peak with cycle number is not inconsistent with replacement of the ions. Another interpretation is that the overshoot is related to water transport.

Skaarup et al. reported an actuation-frequency-dependent strain and proposed that actuation speed depends not only on the transport rate of hydrated ions, but also on the rate of movement of water that is not directly associated with ions due to changes in osmotic pressure as the ion concentrations within the polymer change [21]. The lesson from this transient behavior is that the actuators must be primed under the conditions in which they will be applied, or else ion-exchange phenomena may result in poor control during the initial cycles.

S6. Ramping voltage to attenuate initial transient effects

In section S5, the stepping experiments revealed a transient behavior. To further examine this, the applied voltage was ramped at different rates. Three fresh samples (polymerized together) were first primed by 10 CVs at 25 mV/s in either NaDBS at RT or aCSF at 37 °C. Immediately afterward (in the case of NaDBS-aCSF after transferring to the 2nd electrolyte), the actuators were held at +0.4 V for 100 seconds, ramped down to -1.0 V at 5 mV/s, and then held for 240 seconds. The priming-(transferring)-ramping procedure was repeated at voltage ramps of 50 and 500 mV/s in either NaDBS at RT or aCSF at 37 °C. The beam tip deflections are shown in Sup. Figure 11.



Sup. Figure 11. Deflection as a function of time in response to the voltage profiles shown at the top: samples were held at +0.4 V (oxidized) for 100 seconds, ramped to -1.0 V (reduced) at varying scan rates (5, 50, and 500 mV/s), and then held at -1.0 V for 240 seconds. Priming and ramping electrolytes were either NaDBS at RT or aCSF at 37 °C.

As expected, the bending behavior of the NaDBS-NaDBS sample was similar at the three ramp rates. However, the bending behavior of the NaDBS-aCSF sample depended strongly on the ramp rate, and that of the aCSF-aCSF sample less so.

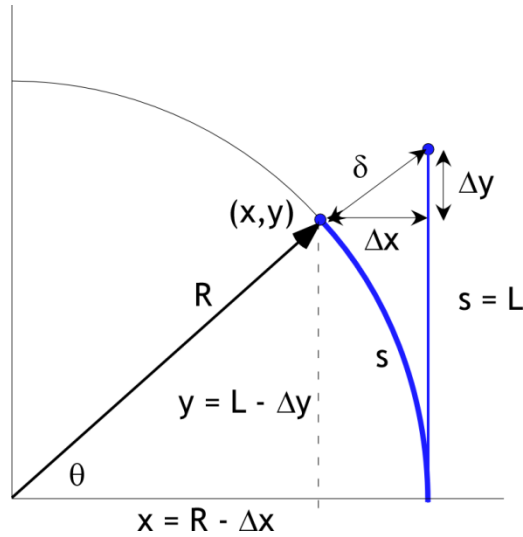
At 5 mV/s, the deflections changed substantially monotonically, although the aCSF-aCSF sample drifted from its maximum deflection to a less curved state over the next 300 seconds, as did the NaDBS-NaDBS sample to a lesser extent. At 50 and 500 mV/s, the tip of the NaDBS-aCSF sample

swung back again instead of remaining still. At 50 mV/s, the tip “overshot” by 1.3 mm beyond the final value (19% of the peak-to-peak value), reversed, and settled to its final position during the first 20 seconds. At 500 mV/s the overshoot was even larger at 2 mm (28% of the final value), but it settled to its final value in about half the time, within 11 sec.

These transients are likely due to multiple ion transport events with different rates, such as the incorporation of ions other than Na⁺ and the expulsion of Na⁺, although we cannot rule out contributions due to the expulsion of water or changes in chain conformation. As discussed in the previous section, transients are undesirable in an application setting. These results motivate future protocols for priming the actuators after deposition in an ionic medium and temperature matching those in the final application. A more thorough investigation would need to be performed to better understand the overshoot phenomenon.

S7. Calculation of curvature and actuation strain from deflection measurements

The curvature of the beam was obtained by trigonometry from the measured Δx and Δy deflections of the beam tip.



Sup. Figure 12. Trigonometry of beam bending used to obtain curvature.

$$(1) \quad \delta = \sqrt{\Delta x^2 + \Delta y^2}$$

$$(2) \quad R^2 = (L - \Delta y)^2 + (R - \Delta x)^2 = (L - \Delta y)^2 + R^2 - 2R\Delta x + \Delta x^2$$

$$(3) \quad R = \frac{(L - \Delta y)^2 + \Delta x^2}{2\Delta x}$$

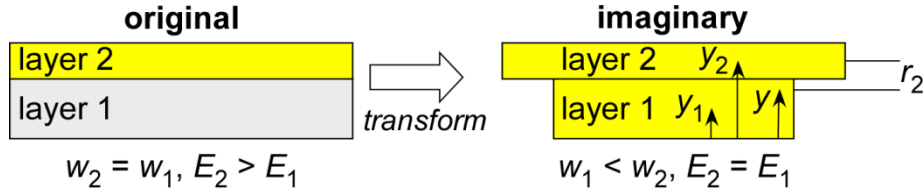
$$(4) \quad \kappa = \frac{1}{R} = \frac{2\Delta x}{(L - \Delta y)^2 + \Delta x^2}$$

S8. Calculation of effective substrate modulus

The bilayer model

$$(5) \quad \kappa = \frac{\alpha_{PPy}}{h_{sub}} \frac{6mn(1+m)}{1+4mn+6m^2n+4m^3n+m^4n^2}$$

was used with an effective modulus E_{sub} for the Parylene+Cr+Au composite substrate. E_{sub} was determined by the transformed section method and the parallel-axis theorem to determine the moment of inertia for a composite area [54, 77]. In the transformed section method, the widths of the layers in the composite beam are adjusted to create an imaginary beam composed of only one material, in our case Au. The layer thicknesses for the Parylene, Cr, and Au were h_{Pa} , h_{Cr} , and h_{Au} respectively. (The beam width w cancels out).



Sup. Figure 13. Beam cross-sections illustrating the transformed section method for a 2-layer beam.

The width ratios are given by n_i :

$$(6) \quad n_1 = \frac{E_{Cr}}{E_{Au}}, \quad n_2 = \frac{E_{Pa}}{E_{Au}} .$$

Next, the parallel-axis theorem is used to determine the moment of inertia for the imaginary beam. The moment of inertia I_{yi} of a layer with respect to the plane going through its center of mass is equal to the moment of inertia I'_{yi} with respect to any parallel plane plus the product of the area A_i and the square of the distance r_i between the two planes. The moment of inertia of a composite beam I_y is the sum of the moments of inertia of all the layers with respect to the same reference plane.

$$(7) \quad I_y = \sum_{i=1}^n I_{yi} = \sum_{i=1}^n I'_{yi} + A_i \cdot r_i^2$$

where $r_i = y_i - y$ and y is the position of the reference plane. We choose to place the reference plane at the centroid (geometric center) of the imaginary beam, a distance y from the bottom of the beam, given by:

$$(8) \quad y = \frac{\sum_{i=1}^n y_i A_i}{\sum_{i=1}^n A_i} = \frac{h_{Au} \left(h_{Cr} + h_{Pa} + \frac{h_{Au}}{2} \right) + n_1 \cdot h_{Cr} \left(h_{Pa} + \frac{h_{Cr}}{2} \right) + n_2 \cdot h_{Pa} \left(\frac{h_{Pa}}{2} \right)}{h_{Au} + n_1 \cdot h_{Cr} + n_2 \cdot h_{Pa}}$$

where y_i is the centroid of each layer and A_i is the cross-sectional area (thickness*width) of each transformed layer.

Substituting Equation (8) for every layer into equation y , I_y is given as:

$$(9) \quad I_y = w \left(\begin{aligned} & \frac{1}{12} h_{Au}^3 + h_{Au} \left(h_{Cr} + h_{Pa} + \frac{h_{Au}}{2} - y \right)^2 + \frac{1}{12} n_1 \cdot h_{Cr}^3 \\ & + n_1 \cdot h_{Cr} \left(h_{Pa} + \frac{h_{Cr}}{2} - y \right)^2 + \frac{1}{12} n_2 \cdot h_{Pa}^3 + n_2 \cdot h_{Pa} \left(y - \frac{h_{Pa}}{2} \right)^2 \end{aligned} \right)$$

The composite substrate equivalent stiffness $(EI)_{sub}$ is obtained by multiplying the Young's modulus E of the reference layer, here E_{Au} , by I_y .

$$(10) \quad (EI)_{sub} = E_{Au} \cdot I_y$$

The moment of inertia of the imaginary beam is I_{sub} .

$$(11) \quad I_{sub} = \frac{1}{12} w \cdot (h_{Au} + h_{Cr} + h_{Pa})^3$$

E_{sub} is finally obtained by dividing the equivalent stiffness $(EI)_{sub}$ by I_{sub} .

$$(12) \quad E_{sub} = \frac{(EI)_{sub}}{I_{sub}}$$

The Young's modulus E_{pa} for Parylene-C was reported by the manufacturer [78] to be 2.76 GPa, but another reports places it between 3.0-3.2 GPa [79] and a third as high as 4.75 GPa [80]. The manufacturer's value was used for this work. The bulk modulus for Au of $E_{Au} = 83$ GPa was used here, although the value for thin film gold has been reported as differing from this [33, 81]. The Cr adhesion layer is generally ignored, but it was thicker than usual on these beams (150 Å) and the Young's modulus E_{Cr} of Cr is high, ranging from 86 GPa up to 279 GPa in bulk Cr [82], so it may significantly contribute to the composite thickness. However, thin film deposited Cr has a reported value of 180 GPa [83]. Therefore, the conservative value of 180 GPa was used for this work. Using these values, the average E_{sub} was 5.07 ± 0.09 GPa. Strains derived from a multiple layer model [84] were compared with those from the bilayer model, and the difference was about 0.3%. The largest uncertainty was contributed by the Parylene layer thicknesses, which were known only to within ± 0.8 μm.

Sup. Table 2. Average actuation strain α , exchanged charge density, and strain-to-charge density (during reduction and oxidation and their sum) in the 9th and 19th scans under different cycling conditions, as well as the ratios of the 19th and 9th scan (n = 3).

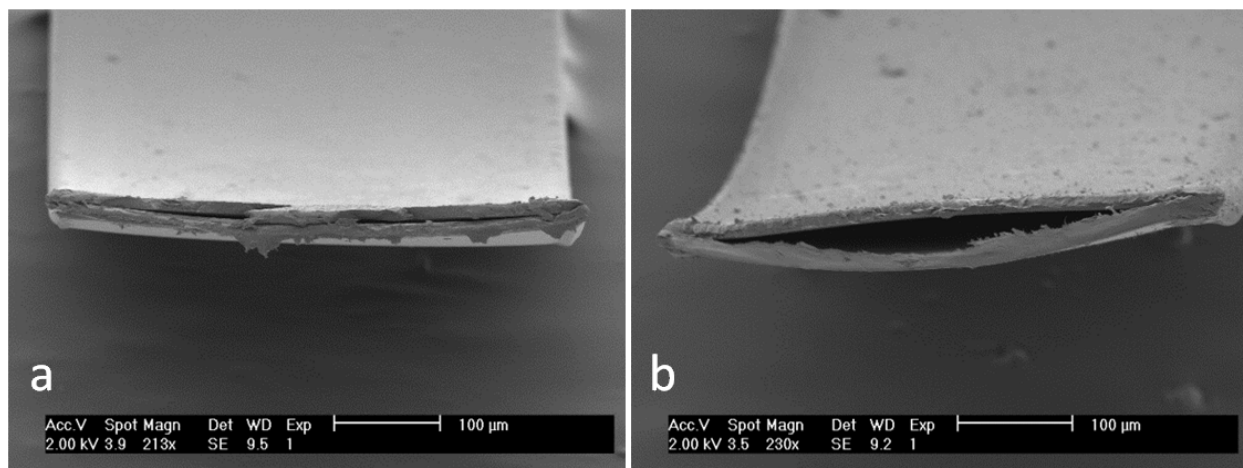
Scan 9		NaDBS RT	NaDBS 37C	aCSF RT	aCSF 37C
α Reduction	%	0.46 ± 0.12	0.34 ± 0.02	0.43 ± 0.11	0.25 ± 0.00
α Oxidation	%	-0.35 ± 0.08	-0.46 ± 0.02	-0.23 ± 0.06	-0.39 ± 0.06
α Total	%	0.81 ± 0.21	0.80 ± 0.02	0.66 ± 0.17	0.64 ± 0.06
Re Charge Density	C/m ³ x 10 ⁶	101 ± 14	102 ± 19	89 ± 17	105*
Ox Charge Density	C/m ³ x 10 ⁶	82 ± 11	85 ± 8	69 ± 13	79*
Total Charge Density	C/m ³ x 10 ⁶	183 ± 24	187 ± 21	158 ± 28	184*
Re α / Charge Density	($\Delta I/I$) / (C/m ³) x 10 ⁻¹²	45.68 ± 13.89	33.24 ± 6.57	48.70 ± 15.35	23.35 ± 0.47
Ox α / Charge Density	($\Delta I/I$) / (C/m ³) x 10 ⁻¹²	-42.81 ± 11.47	-53.70 ± 5.76	-33.08 ± 10.88	-49.88 ± 7.66
Tot α / Charge Density	($\Delta I/I$) / (C/m ³) x 10 ⁻¹²	44.40 ± 12.64	42.54 ± 4.95	41.88 ± 13.08	34.74 ± 3.47

Scan 19		NaDBS RT	NaDBS 37C	aCSF RT	aCSF 37C
α Reduction	%	0.50 ± 0.14	0.20 ± 0.03	0.37 ± 0.11	0.10 ± 0.07
α Oxidation	%	-0.32 ± 0.13	-0.70 ± 0.07	-0.21 ± 0.04	-0.50 ± 0.04
α Total	%	0.83 ± 0.25	0.90 ± 0.07	0.59 ± 0.15	0.60 ± 0.11
Re Charge Density	C/m ³ x 10 ⁶	112 ± 9	182 ± 26	91 ± 4	176*
Ox Charge Density	C/m ³ x 10 ⁶	87 ± 13	133 ± 18	70 ± 2	135*
Total Charge Density	C/m ³ x 10 ⁶	199 ± 21	311 ± 44	161 ± 22	312*
Re α / Charge Density	($\Delta I/I$) / (C/m ³) x 10 ⁻¹²	45.03 ± 13.36	10.84 ± 2.10	41.08 ± 12.08	5.56 ± 3.86
Ox α / Charge Density	($\Delta I/I$) / (C/m ³) x 10 ⁻¹²	-37.34 ± 15.60	-52.61 ± 9.05	-30.47 ± 5.67	-37.26 ± 3.21
Tot α / Charge Density	($\Delta I/I$) / (C/m ³) x 10 ⁻¹²	41.67 ± 13.43	28.84 ± 4.59	36.47 ± 10.45	19.26 ± 3.49

Ratio of Scans 19/9		NaDBS RT	NaDBS 37C	aCSF RT	aCSF 37C
α Reduction		1.09 ± 0.43	0.58 ± 0.09	0.86 ± 0.33	0.40 ± 0.28
α Oxidation		0.93 ± 0.42	1.53 ± 0.18	0.93 ± 0.31	1.28 ± 0.22
α Total		1.02 ± 0.40	1.13 ± 0.09	0.89 ± 0.32	0.94 ± 0.19
Re Charge Density		1.11 ± 0.18	1.78 ± 0.42	1.02 ± 0.20	1.68*
Ox Charge Density		1.06 ± 0.21	1.56 ± 0.26	1.01 ± 0.19	1.71*
Total Charge Density		1.09 ± 0.18	1.66 ± 0.30	1.02 ± 0.23	1.70*
Re α / Charge Density		0.99 ± 0.42	0.33 ± 0.09	0.84 ± 0.36	0.24 ± 0.17
Ox α / Charge Density		0.87 ± 0.43	0.98 ± 0.20	0.92 ± 0.35	0.75 ± 0.13
Tot α / Charge Density		0.94 ± 0.40	0.68 ± 0.13	0.87 ± 0.37	0.55 ± 0.11

* Denotes data from one sample.

S9. Cross-sectional images of devices showing delamination



Sup. Figure 14. SEM images of bilayer cross sections of devices after being cut mid-length with some samples showing (a) no delamination and (b) delamination of the PPy layer. The delamination may have occurred during actuation or due to cutting.

In order to quantify the layer thicknesses, devices were cut using a razor blade midway along the length of the beam. Images of the cross-section of many of the devices showed signs of delamination, such as in Sup. Figure 14b. Delamination during actuation may explain the shifts in repeated CV current peaks as seen in S3, however, it is difficult to distinguish when the separation occurred.